



Extensive spatiotemporal analyses of surface ozone and related meteorological variables in South Korea for the period 1999–2010

J. Seo^{1,3}, D. Youn², J. Y. Kim¹, and H. Lee⁴

¹Green City Technology Institute, Korea Institute of Science and Technology, Seoul, South Korea

²Department of Earth Science Education, Chungbuk National University, Cheongju, South Korea

³School of Earth and Environmental Sciences, Seoul National University, Seoul, South Korea

⁴Jet Propulsion Laboratory, California Institute of Technology, Pasadena, CA, USA

Correspondence to: D. Youn (dyoun@chungbuk.ac.kr)

Received: 22 November 2013 – Published in Atmos. Chem. Phys. Discuss.: 15 January 2014

Revised: 25 April 2014 – Accepted: 14 May 2014 – Published: 26 June 2014

Abstract. Spatiotemporal characteristics of surface ozone (O_3) variations over South Korea are investigated with consideration of meteorological factors and timescales based on the Kolmogorov–Zurbenko filter (KZ filter), using measurement data at 124 air quality monitoring sites and 72 weather stations for the 12 yr period of 1999–2010. In general, O_3 levels at coastal cities are high due to dynamic effects of the sea breeze while those at the inland and Seoul Metropolitan Area (SMA) cities are low due to the NO_x titration by local precursor emissions. We examine the meteorological influences on O_3 using a combined analysis of the KZ filter and linear regressions between O_3 and meteorological variables. We decomposed O_3 time series at each site into short-term, seasonal, and long-term components by the KZ filter and regressed on meteorological variables. Impact of temperature on the O_3 levels is significantly high in the highly populated SMA and inland region, but low in the coastal region. In particular, the probability of high O_3 occurrence doubles with 4 °C of temperature increase in the SMA during high O_3 months (May–October). This implies that those regions will experience frequent high O_3 events in a future warming climate. In terms of short-term variation, the distribution of high O_3 probability classified by wind direction shows the effect of both local precursor emissions and long-range transport from China. In terms of long-term variation, the O_3 concentrations have increased by +0.26 ppbv yr⁻¹ (parts per billion by volume) on nationwide average, but their trends show large spatial variability. Singular value decomposition analyses further reveal that the long-term temporal evolution of O_3 is similar to that of nitrogen dioxide, although the spa-

tial distribution of their trends is different. This study will be helpful as a reference for diagnostics and evaluation of regional- and local-scale O_3 and climate simulations, and as a guide to appropriate O_3 control policy in South Korea.

1 Introduction

Surface ozone (O_3) is a well-known secondary air pollutant, which affects air quality, human health, and vegetation. High O_3 concentrations have detrimental effects on respiration, lung function, and airway reactivity in human health (Bernard et al., 2001; Bell et al., 2007). In terms of mortality, Levy et al. (2005) have previously assessed that a 10 ppbv (parts per billion by volume) increase in 1 h maximum O_3 could increase daily mortality by 0.41 %. High O_3 concentrations could also reduce agricultural production. For example, Wang and Mauzerall (2004) reported that the East Asian countries of China, Japan, and South Korea lost 1–9 % of their yields of wheat, rice, and corn, and 23–27 % of their yields of soybeans due to O_3 in 1990. In addition, O_3 is one of the greenhouse gases for which radiative forcing is estimated as the third largest contribution among the various constituents in the troposphere (IPCC, 2007). Therefore, the spatially inhomogeneous distribution of O_3 due to its short chemical lifetime of a week to a month could induce strong regional-scale climate responses (Mickley et al., 2004).

In the Northern Hemisphere midlatitudes where population, industry, and transportation are concentrated, the background O_3 levels increased during the late-20th century due

to increases in anthropogenic precursors particularly nitrogen oxides (NO_x), but its trends show regional and temporal differences (Oltmans et al., 1998; Guicherit and Roemer, 2000; Vingarzan, 2004). Although the increasing trends of O_3 in Europe, the North Atlantic, North America, and Japan have flattened over the past decade (Oltmans et al., 2006, 2013), there have still been concerns about elevated O_3 concentrations in China owing to rapid economic growth and industrialization (Ding et al., 2008; Tang et al., 2009; Wang et al., 2009, 2012). Such recent increases of O_3 in China can affect the regional background O_3 levels in East Asia by transboundary transport of O_3 and its precursors. For example, previous modeling studies have shown that the transport of O_3 from China by continental outflow is one of the major contributions of O_3 in Japan and South Korea (Tanimoto et al., 2005; Nagashima et al., 2010). Intercontinental transport of O_3 and its precursors originated in East Asia affects O_3 concentrations and air quality in remote areas even on a global scale (Akimoto, 2003). Experiments using a global climate-chemistry model with future emission scenarios by Lei et al. (2013) suggest that the increase in East Asian emissions will still be an important issue for the O_3 air quality in both East Asia and the United States.

Recently, several studies have focused on the relationship between O_3 levels and temperature, and suggested potential influences of the global warming and climate change on the high levels of O_3 (Jacob and Winner, 2009; Rasmussen et al., 2012, and references therein). Lin et al. (2001) calculated probability of daily maximum 8 h average O_3 exceeding 85 ppbv for a given range of daily maximum temperatures and reported that a 3 °C increase of the daily maximum temperature doubles risk of O_3 exceedances in the northeastern United States. In addition, Ordóñez et al. (2005) showed that high temperature extremes probably led to the high occurrence of severe O_3 episodes during the summer 2003 heat wave over Europe. These results imply the potentially large sensitivity of O_3 concentration and related air quality to the temperature increases (Jacob and Winner, 2009). In the model experiments by Lin et al. (2008), both averaged O_3 concentrations and frequencies of high O_3 episodes were predicted to increase in future over the United States and East Asia. Recent global climate-chemistry model experiments by Lei and Wang (2014) also implied the future O_3 increases in industrial regions due to more O_3 production by photochemical reactions and less O_3 removal by nocturnal odd nitrogen (NO_y) chemistry in warmer conditions.

In South Korea, one of the most densely populated countries in the world, both O_3 concentrations and high O_3 episodes have increased in recent decades despite efforts to regulate emissions of O_3 precursors (KMOE, 2012). Although the increase of O_3 levels in South Korea over the last 3 decades is mainly regarded as the results of rapid industrialization, economic expansion, and urbanization, there are other factors to be considered to explain the long-term increase in O_3 concentrations. For example, since the Ko-

rean Peninsula is located on the eastern boundary of East Asia, downward transport of O_3 by the continental outflow considerably affects the high O_3 levels in South Korea (Oh et al., 2010). In addition, a recent warming trend related to global climate change could also be an important factor to increase O_3 concentrations in South Korea. Climate change is expected to increase both frequency and intensity of temperature extremes over the Korean Peninsula (Boo et al., 2006). Therefore, comprehensive understanding of the various factors affecting O_3 concentrations, such as local precursor emissions, transport of O_3 and its precursors from local and remote sources, and changes in meteorological fields related to climate change is required to guide environmental policies.

The present study aims to examine the spatiotemporal characteristics of the measured O_3 variations in South Korea with consideration of three timescales and various meteorological factors, using ground-measured data from 124 air quality monitoring sites and 72 weather stations for the 12 yr period of 1999–2010. We decomposed O_3 time series at each measurement site into different timescales of short-term, seasonal, and long-term components by application of the Kolmogorov–Zurbenko filter (KZ filter) that has been used in previous studies (e.g., Gardner and Dorling, 2000; Ibarra-Berastegi et al., 2001; Thompson et al., 2001; Lu and Chang, 2005; Wise and Comrie, 2005; Tsakiri and Zurbenko, 2011; Shin et al., 2012). To investigate the meteorological impact on the O_3 levels, we applied the combined analysis of the KZ filter and linear regression model with the meteorological variables. In the short-term timescale, the possible effects of transport from the local and remote sources on the high O_3 episodes were explored by using the wind data. In the long-term timescale, the singular value decomposition (SVD) with nitrogen dioxide (NO_2) measurements was additionally applied to examine the effects of varying local emissions on the long-term O_3 trend.

The remainder of this paper is structured as follows. In the next section, we describe the observational data and analysis techniques used in this study. In Sect. 3, we investigate the spatiotemporal characteristics of the decomposed O_3 time series and its relationship with meteorological variables over South Korea. Finally, the key findings are summarized in Sect. 4.

2 Data and methodologies

2.1 Data

The National Institute of Environmental Research (NIER) of South Korea provides hourly data of O_3 and NO_2 mixing ratios in the ppbv unit, which have been measured by ultraviolet absorption and chemiluminescence, respectively. We here select 124 urban air quality monitoring sites over South Korea, based on data availability for the period 1999–2010, and

analyze hourly time series of O_3 and NO_2 from each site. It is noted that our current analyses exclude other data from roadside measurement sites where data can be directly affected by the vehicle exhaust emissions and suburban and background sites located around South Korea. Hourly meteorological data at 72 weather stations of the Korea Meteorological Administration (KMA) for the same period are also used to examine the effects of meteorological factors on the O_3 variations. The meteorological variables used in this study include common factors related to the O_3 variations such as temperature ($^{\circ}C$), surface insolation ($W\ m^{-2}$), relative humidity (%), and wind speed ($m\ s^{-1}$) (e.g., Ordóñez et al., 2005; Camalier et al., 2007; Jacob and Winner, 2009). Dew-point temperature ($^{\circ}C$) and sea-level pressure (hPa) are additionally applied for multiple linear regression models as other previous studies have done (e.g., Thompson et al., 2001; Shin et al., 2012). Finally, wind direction (16 cardinal directions) is used to reveal its relationship with short-term changes in O_3 . Using the hourly data, we first calculated daily averages for O_3 ($O_{3\text{avg}}$), NO_2 ($NO_{2\text{avg}}$), temperature (T), surface insolation (SI), dew-point temperature (TD), sea-level pressure (PS), wind speed (WS), wind direction (WD), and relative humidity (RH). We also obtained daily minimum O_3 ($O_{3\text{min}}$), daily maximum 8 h average O_3 ($O_{3\text{8h}}$), and daily maximum temperature (T_{max}) from the hourly data set.

To investigate the relationship between O_3 and meteorological variables, it is desirable to use data observed at the same stations. However, not all air quality monitoring sites and weather stations are closely located in South Korea. Therefore, we assume that an air quality monitoring site can observe the same meteorological variables as those at a weather station if the distance between the two places is less than 10 km. Under this assumption, only O_3 data from 72 air quality monitoring sites and meteorological data from 25 weather stations are available to analyze the meteorological effects on the O_3 variation over South Korea. The insolation was measured only at 17 weather stations for the analysis period. Figure 1 shows geographical locations of the ground measurements used in the present study, together with colored topography based on the US Geological Survey (USGS) digital elevation model (DEM).

2.2 Decomposition of O_3 time series by KZ filter

The KZ filter is a decomposition method that can be used to separate time series into short-term, seasonal, and long-term components (Rao and Zurbenko, 1994). We applied the KZ filter to the O_3 time series by taking the moving average of window length m with iterating p times, which is denoted by $KZ_{m,p}$. The KZ filter is basically a low-pass filter for removing high-frequency components from the original time series. Following Eskridge et al. (1997), the KZ filter removes the signal smaller than the period N , which is called as the ef-

fective filter width. N is defined as follows:

$$m \times p^{1/2} \leq N. \quad (1)$$

The KZ-filter method has the same level of accuracy as the wavelet transform method although it is a much easier way to decompose the original time series (Eskridge et al., 1997). In addition, time series with missing observations can be applicable to the KZ filter owing to the iterative moving average process.

For the clear separation of the components, we applied the KZ filter to the daily log-transformed O_3 as in Rao and Zurbenko (1994) and Eskridge et al. (1997), instead of the raw O_3 concentrations. While the short-term component separated by the KZ filter using raw O_3 data still shows clear seasonality, use of $\ln(O_3)$ makes the short-term component stationary and nearly independent of the seasonal influence by stabilizing variance (Rao and Zurbenko, 1994; Rao et al., 1997). Note that a temporal linear trend of log-transformed data is provided as percent per year ($\% \text{ yr}^{-1}$) because the differential of the natural logarithm is equivalent to the percentage change.

The natural logarithm of the O_3 time series at each site denoted as $[O_3](t)$ is thus decomposed by the KZ filter as follows:

$$[O_3](t) = [O_{3\text{ST}}](t) + [O_{3\text{SEASON}}](t) + [O_{3\text{LT}}](t). \quad (2)$$

$[O_{3\text{ST}}]$ is a short-term component attributable to day-to-day variation of synoptic-scale weather and short-term fluctuation in precursor emissions. $[O_{3\text{SEASON}}]$ represents a seasonal component related to the seasonal changes in solar radiation and vertical transport of O_3 from the stratosphere whose timescale is from several weeks to months. $[O_{3\text{LT}}]$ denotes a long-term component explained by changes in precursor emission, transport, climate, policy, and economy over the entire period (Rao et al., 1997; Milanchus et al., 1998; Gardner and Dorling, 2000; Thompson et al., 2001; Wise and Comrie, 2005). Tsakiri and Zurbenko (2011) showed that $[O_{3\text{ST}}]$ and $[O_{3\text{LT}}]$ are independent of each other. Also, statistical characteristics of $[O_{3\text{ST}}]$ are very close to those of white noise (Flaum et al., 1996) and therefore $[O_{3\text{ST}}]$ is nearly detrended.

In this study, we used the KZ filter with the window length of 29 days and 3 iterations ($KZ_{29,3}$) following previous studies (e.g., Rao and Zurbenko, 1994) and decomposed daily $\ln(O_{3\text{8h}})$ time series at the 124 monitoring sites. $KZ_{29,3}$ removes the $[O_{3\text{ST}}]$ with period shorter than about 50 days, following Eq. (1). We defined the filtered time series as a baseline ($[O_{3\text{BL}}]$) as in Eq. (3).

$$[O_3](t) = [O_{3\text{BL}}](t) + [O_{3\text{ST}}](t) \quad (3)$$

Equation (3) accounts for the multiplicative effects of short-term fluctuations on the $[O_{3\text{BL}}]$ due to the log transformation (Thompson et al., 2001). In other words, the exponential of

$[O_{3ST}]$ is a ratio of the raw O_3 concentrations to the exponential of $[O_{3BL}]$, which is the baseline O_3 concentration in ppbv. Therefore, if $\exp[O_{3ST}]$ is larger than 1, the raw O_3 concentration will be larger than the baseline O_3 concentration.

$[O_{3BL}]$ is expressed as the sum of $[O_{3SEASON}]$ and $[O_{3LT}]$, as in Eq. (4) (Milanchus et al., 1998).

$$[O_{3BL}](t) = [O_{3SEASON}](t) + [O_{3LT}](t) \quad (4)$$

Since $[O_{3BL}]$ is closely associated with meteorological fields, we built a multiple regression model with available meteorological variables as in Eq. (5), following previous studies (e.g., Rao and Zurbenko, 1994; Rao et al., 1995; Ibarra-Berastegi et al., 2001). Short-term variability of meteorological variables was also filtered out by $KZ_{29,3}$.

$$[O_{3BL}](t) = a_0 + \sum_i a_i MET_{BL}(t)_i + \varepsilon(t)$$

$$MET_{BL}(t) = [T_{maxBL}(t), SI_{BL}(t), TD_{BL}(t),$$

$$PS_{BL}(t), WS_{BL}(t), RH_{BL}(t)] \quad (5)$$

In the multiple linear regression model, $[O_{3BL}]$ is a response variable and the baselines of meteorological variables ($MET_{BL}(t)_i$) are predictors. Also, a_0 , a_i , and $\varepsilon(t)$ denote the constant, regression coefficient of variable i , and residual of the multiple regression model, respectively.

The residual term $\varepsilon(t)$ contains not only the long-term variability of O_3 related to long-term changes in local precursor emissions but also seasonal variability of O_3 attributable to unconsidered meteorological factors in the multiple linear regression model. Thus, we applied the KZ filter with the window length of 365 days and 3 iterations ($KZ_{365,3}$) to $\varepsilon(t)$ to extract the meteorologically adjusted $[O_{3LT}]$ of which the period is larger than about 1.7 yr as follows:

$$\varepsilon(t) = KZ_{365,3}[\varepsilon(t)] + \delta(t) = [O_{3LT}](t) + \delta(t). \quad (6)$$

In Eq. (6), $\delta(t)$ denotes the seasonal variability of O_3 related to the meteorological variables unconsidered in the multiple linear regression model and/or noise.

Finally, $[O_{3SEASON}]$ is obtained by sum of the combined meteorological variables regressed on $[O_{3BL}]$ ($a_0 + \sum_i a_i MET_{BL}(t)_i$) and $\delta(t)$ as in Eq. (7).

$$[O_{3SEASON}](t) = a_0 + \sum_i a_i MET_{BL}(t)_i + \delta(t) \quad (7)$$

Figure 2 shows a schematic representation of Eq. (2) using daily O_{38h} time series at the City Hall of Seoul for the period of 1999–2010. $[O_{3SEASON}]$ in Fig. 2c clearly shows the typical seasonal cycle of O_3 in South Korea with high concentrations in spring, slight decrease in July and August, and increase in autumn (Ghim and Chang, 2000). The spring maximum of O_3 concentration in the Northern Hemisphere is generally attributed to episodic stratospheric intrusion (Levy et

al., 1985; Logan, 1985), photochemical reactions of accumulated NO_x and hydrocarbons during the winter (Dibb et al., 2003), accumulation of O_3 due to the longer photochemical lifetime (~ 200 days) during the winter (Liu et al., 1987), and transport of O_3 and its precursors by the continental outflow (Carmichael et al., 1998; Jacob et al., 1999; Jaffe et al., 2003). However, frequent precipitation during the East Asian summer monsoon influences the decrease of O_3 concentrations in July and August (Ghim and Chang, 2000). $[O_{3LT}]$ in Fig. 2d shows that the O_3 concentrations at the monitoring site have increased in the past decade, irrespective of any change in meteorological conditions. It should be noted that $[O_{3LT}]$ explains only 1.7 % of the total variance of $[O_3]$ at this site as can be seen from its small ranges in Fig. 2d, while relative contributions of $[O_{3ST}]$ and $[O_{3SEASON}]$ are 58.3 and 32.7 %, respectively. Therefore, the long-term changes in O_3 related to changes in local emission are only a small fraction of the O_3 variations. The relative contributions of each component are further examined in Sect. 3.4.

2.3 Spatial interpolation by AIDW method

Inverse-distance weighting (IDW) is a deterministic spatial interpolation technique for spatial mapping of variables distributed at irregular points. In this study, we adopted the enhanced version of the IDW, the adaptive inverse-distance weighting (AIDW) technique (Lu and Wong, 2008). While the traditional IDW uses a fixed distance-decay parameter without considering the distribution of data within it, the AIDW uses adjusted distance-decay parameters according to density of local sampling points. Therefore, the AIDW provides flexibility to accommodate variability in the distance-decay relationship over the domain and thus better spatial mapping of variables distributed at irregular observational points (Lu and Wong, 2008).

In the mapping of O_3 with spatial interpolation, there are ubiquitous problems such as spatial-scale violations, improper evaluations, inaccuracy, and inappropriate use of O_3 maps in certain analyses (Diem, 2003). The spatial mapping in the present study also has problems with the spatial resolution of the observations, which is not high enough to consider small-scale chemical processes and the geographical complexity of the Korean Peninsula (see Fig. 1). Most of the air quality monitoring sites are concentrated on the cities, and typical intercity distances are 30–100 km in South Korea while spatial representativeness of O_3 concentrations is possibly as small as around 3–4 (Tilmes and Zimmermann, 1998) or 5 km (Diem, 2003). In addition, mapping with a few monitoring sites combined with complex mountainous terrain can also distort the actual distribution of data, especially in the northeastern part of South Korea. Despite such limits, the spatial mapping in this study is still useful because we aim not to derive an exact value at a specific point where the observation does not exist, but to provide the better quantitative understanding of O_3 and related factors in South

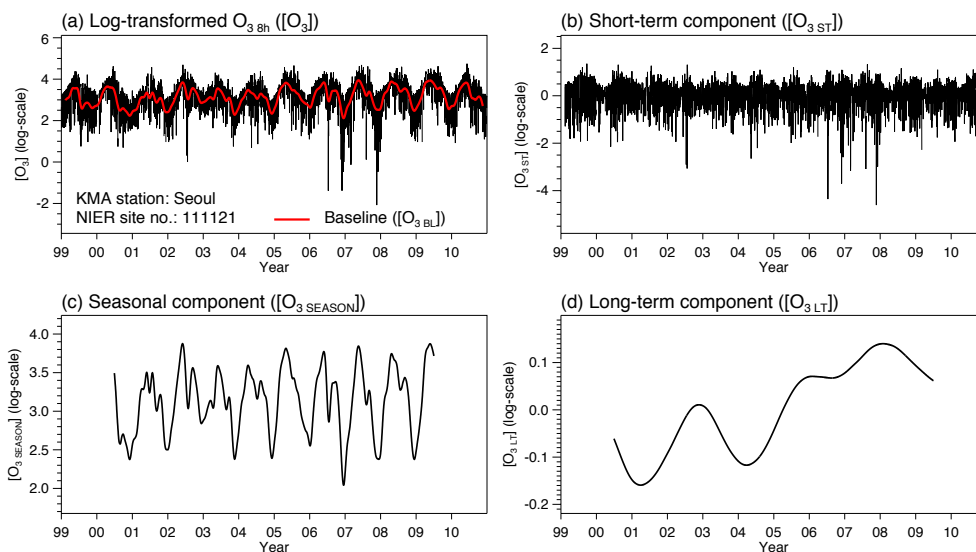


Figure 1. Time series of daily maximum 8 h average ozone ($O_{3, 8h}$) at the City Hall of Seoul and its separated components such as (a) log-transformed $O_{3, 8h}$ time series ($[O_3]$) and its baseline ($[O_{3, BL}]$), (b) short-term component ($[O_{3, ST}]$), (c) seasonal component ($[O_{3, SEASON}]$), and (d) long-term component ($[O_{3, LT}]$) by applying the KZ filter. It is noted that the longer window length causes the larger truncation of the result (Wise and Comrie, 2005) since the KZ filter is an iterative moving average process. The baseline (red solid line) is superimposed in (a).

Korea, especially focused on the metropolitan and urban areas.

3 Results

3.1 Spatial characteristics of O_3 and its trend in South Korea

Climatological daily average O_3 ($O_{3, avg}$) and its temporal linear trends are represented in Fig. 3 and Table 1 using data from 124 monitoring sites distributed nationwide in 46 cities for the past 12 yr period. The spatial map of climatological daily average NO_2 ($NO_{2, avg}$) is also shown in Fig. 3. In Table 1, the cities are categorized into three geographical groups: 16 coastal cities, 14 inland cities, and 16 cities in the Seoul Metropolitan Area (SMA). We separated the SMA cities from the other two groups since the SMA is the largest source region of anthropogenic O_3 precursors in South Korea. The SMA occupies only 11.8 % (11 745 km²) of the national area, but has 49 % (25.4 million) of the total population and 45 % (8.1 million) of total vehicles in South Korea. It is estimated that approximately 27 % (0.29 Mt) of total NO_x emissions and 34 % (0.30 Mt) of the volatile organic compound (VOC) emissions in South Korea were from the SMA in 2010 (KMOE, 2013). Therefore, the climatological $NO_{2, avg}$ concentration in the SMA is much higher than that in other regions (Fig. 3b).

In general, O_3 concentrations are high at the coastal cities, low at the inland cities, and lowest at the SMA cities in South Korea. Along with Table 1, Fig. 3a shows that the 12 yr aver-

age of $O_{3, avg}$ is high at the southern coastal cities such as Jinhae (31.3 ppbv), Mokpo (30.3 ppbv), and Yeosu (28.1 ppbv), with the highest value at Jeju (32.6 ppbv), and low at the inland metropolitan cities such as Daegu (19.8 ppbv), Gwangju (20.5 ppbv), and Daejeon (20.7 ppbv), with lowest values at the SMA cities including Seoul (17.1 ppbv), Incheon (19.0 ppbv) and Anyang (16.8 ppbv).

Compared to the regional background concentration of 35–45 ppbv at five background measurement sites around South Korea (KMOE, 2012), the averaged O_3 concentrations in the SMA and inland metropolitan cities are much lower while those at the coastal cities are close to the regional background levels. In comparison with Fig. 3b, Fig. 3a shows that relatively lower $O_{3, avg}$ regions are well consistent with relatively higher $NO_{2, avg}$ regions. Substantial emissions of anthropogenic NO in the SMA and other inland metropolitan cities lead to NO_x titration effects even in the absence of photochemical reactions during the night, and thus the averaged O_3 concentrations are depressed by 10–20 ppbv lower than the regional background concentration (Ghim and Chang, 2000). A recent modeling study by Jin et al. (2012) has suggested that the maximum O_3 concentrations in the SMA, especially in Seoul and Incheon, are VOC-limited. In the coastal region, however, low emissions of NO with dilution by the strong winds weaken the titration effect and result in the high O_3 concentrations. The dynamic effect of land–sea breeze is another possible factor of the high O_3 levels at the coastal cities. Oh et al. (2006) showed that a near-stagnant wind condition at the development of sea breeze temporarily contains O_3 precursors carried by the offshore land breeze

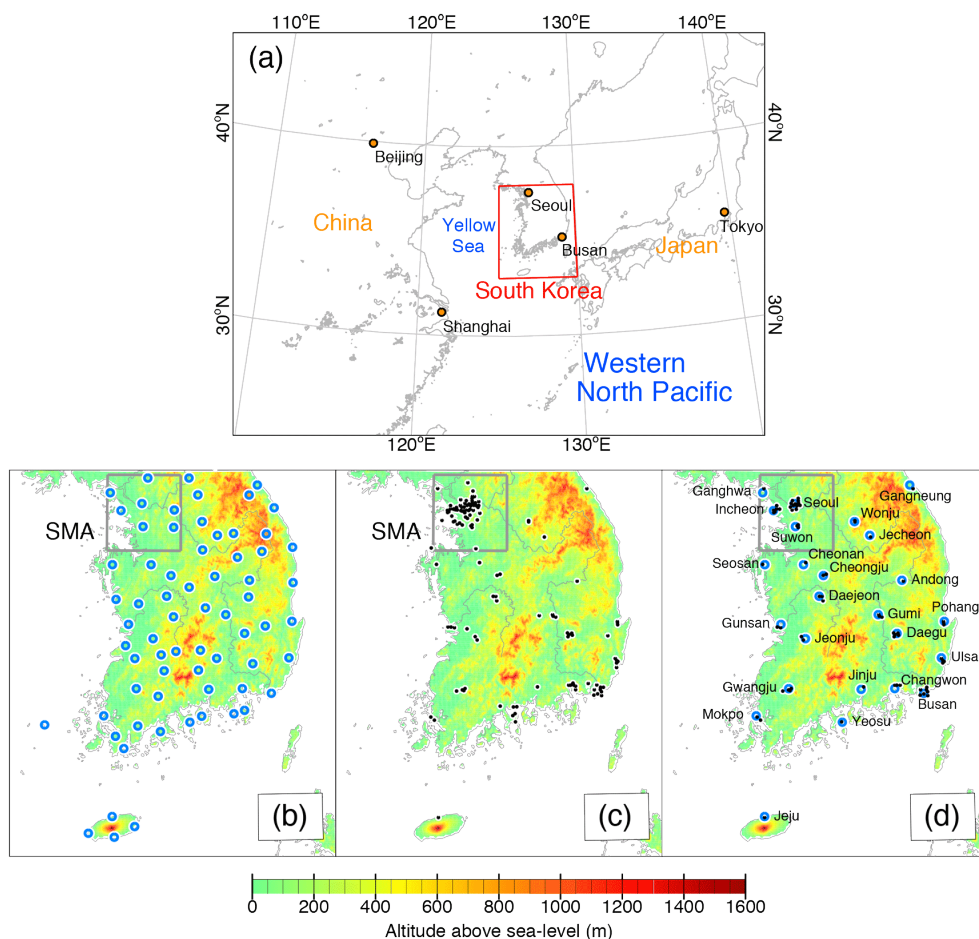


Figure 2. (a) Geographical location of South Korea, (b) 72 weather stations of the Korea Meteorological Administration (KMA) as blue circles, (c) 124 air quality monitoring sites of the National Institute of Environmental Research (NIER) as black dots, and (d) 72 air quality monitoring sites of NIER, which are located within 10 km from 25 weather stations of KMA over the South Korean domain.

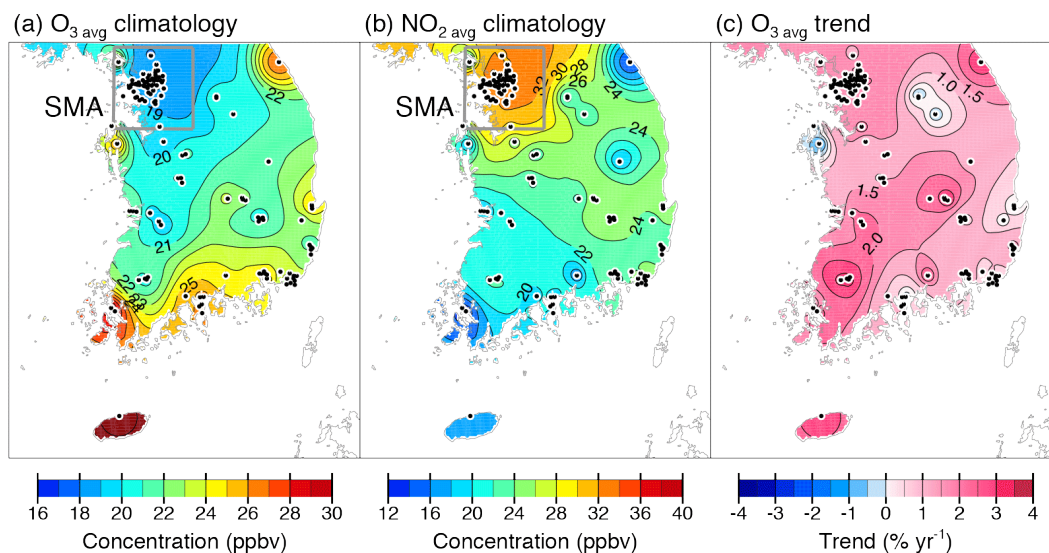


Figure 3. Spatial distributions of 12 yr averaged concentrations of (a) daily average O_3 ($O_{3\text{avg}}$), (b) daily average nitrogen dioxide ($NO_{2\text{avg}}$), and (c) temporal linear trends of $O_{3\text{avg}}$ for the period 1999–2010 using data from 124 air quality monitoring sites (black dots) of NIER.

Table 1. 12 yr averaged concentrations and temporal linear trends of daily average O₃ (O_{3,avg}) at 46 cities over South Korea for the period 1999–2010. The cities are categorized into three groups: 16 coastal cities, 14 inland cities, and 16 cities in the SMA.

Coastal region	City code	O _{3,avg} (ppbv)	Trend (% yr ⁻¹)	Inland region	City code	O _{3,avg} (ppbv)	Trend (% yr ⁻¹)	SMA	City code	O _{3,avg} (ppbv)	Trend (% yr ⁻¹)
Busan*	BS	23.2	0.65	Andong	AD	22.0	1.35	Ansan	–	20.5	1.81
Changwon	CW	25.1	1.62	Cheonan	CN	18.7	0.72	Anyang	–	16.8	0.67
Gangneung	GN	26.5	2.61	Cheongju	CJ	21.0	1.25	Bucheon	–	18.3	1.71
Gimhae	–	24.4	-0.05	Daegu*	DG	19.8	0.77	Ganghwa	GH	30.9	1.12
Gunsan	GS	22.5	0.66	Daejeon*	DJ	20.7	1.21	Goyang	–	19.1	0.77
Gwangyang	–	28.1	-1.28	Gimcheon	–	24.4	2.36	Gunpo	–	19.6	-0.86
Jeju	JJ1	32.6	2.59	Gumi	GM	22.6	3.70	Guri	–	18.1	-0.83
Jinhae	–	31.3	1.03	Gwangju*	GJ	20.5	3.50	Gwacheon	–	17.6	-1.25
Masan	–	25.2	0.85	Gyeongju	–	22.1	-0.27	Gwangmyeong	–	18.0	0.41
Mokpo	MP	30.3	-0.21	Iksan	–	17.7	2.64	Incheon*	IC	19.0	1.45
Pohang	PH	25.7	0.01	Jecheon	JC	21.0	-0.21	Pyeongtaek	–	19.9	2.75
Seosan	SS	27.5	-1.67	Jeonju	JJ2	18.9	2.55	Seongnam	–	18.8	0.66
Suncheon	–	25.7	0.92	Jinju	JJ3	24.0	2.54	Seoul*	SU	17.1	2.82
Ulsan*	US	21.5	1.61	Wonju	WJ	20.7	-0.24	Siheung	–	21.0	2.29
Yeongam	–	28.6	3.58					Suwon	SW	19.3	1.86
Yeosu	YS	28.1	1.18					Uijeongbu	–	19.9	1.46
Coastal averages		26.6	0.88	Inland averages		21.0	1.56	SMA averages		19.6	1.05
Nationwide averages		22.5	1.15								

* Major metropolitan cities in South Korea (Seoul, Busan, Daegu, Incheon, Gwangju, Daejeon, and Ulsan).

during the night, and following photochemical reactions at midday produces O₃. The relationship between O₃ and wind speed and direction will be shown in Sects. 3.2 and 3.5, respectively.

In terms of temporal trends, the surface O₃ concentrations in South Korea have generally increased for the past 12 yr as shown in Fig. 3c and Table 1. The averaged temporal linear trend of O_{3,avg} at 46 cities nationwide is +1.15 % yr⁻¹ (+0.26 ppbv yr⁻¹), which is comparable with observed increasing trends of approximately +0.5–2 % yr⁻¹ in various regions in the Northern Hemisphere (Vingarzan, 2004). Compared with previous studies in East Asia, the overall increasing trend of O₃ in South Korea is smaller than recent increasing trends over China of +1.1 ppbv yr⁻¹ in Beijing for the period 2001–2006 (Tang et al., 2009) and +0.58 ppbv yr⁻¹ in Hong Kong for the period 1994–2007 (Wang et al., 2009) but slightly larger than increasing trend over Japanese populated areas of +0.18 ppbv yr⁻¹ for 1996–2005 (Chatani and Sudo, 2011).

Several factors that could influence the overall increase of O₃ over East Asia were suggested by the following previous studies. Recently, Zhao et al. (2013) have estimated that the NO_x emissions in China increased rapidly from 11.0 Mt in 1995 to 26.1 Mt in 2010, mainly due to the fast growth of energy consumption. The NO_x and VOC emissions in South Korea also increased in the early 2000s. The estimated anthropogenic NO_x and VOC emissions are 1.10 and 0.74 Mt in 1999 but 1.35 and 0.87 Mt in 2006, respectively (KMOE,

2013). Tanimoto et al. (2009) suggested that the O₃ increase results from such recently increased anthropogenic precursor emissions in East Asia.

However, model sensitivity simulations in Chatani and Sudo (2011) indicate that the changes in East Asian emissions can explain only 30 % of the O₃ trend. They have suggested the long-term variations in meteorological fields as a possible important factor although further studies are required. In particular, it is well known that insolation and temperature are important meteorological factors in O₃ variation. While insolation directly affects O₃ production through photochemical reactions, increased temperature affects net O₃ production rather indirectly by increasing biogenic hydrocarbon emissions, hydroxyl radical (OH) with more evaporation, and NO_x and HO_x radicals by thermal decomposition of the peroxyacetyl nitrate (PAN) reservoir (Sillman and Samson, 1995; Olszyna et al., 1997; Racherla and Adams, 2006; Dawson et al., 2007). Therefore, the O₃ increasing trend in Fig. 3c is possibly affected by changes in meteorological variables.

Figure 4 shows temporal linear trends of daily average temperature (*T*) and insolation (*SI*). Despite the spatial discrepancy between trends of O₃ (Fig. 3c) and meteorological variables (Fig. 4), both temperature and insolation have generally increased in South Korea for the past 12 yr. The spatial mean of the temporal linear trend in temperature at 72 weather stations nationwide is approximately +0.09 °C yr⁻¹, which is much higher than +0.03 °C yr⁻¹ for the Northern

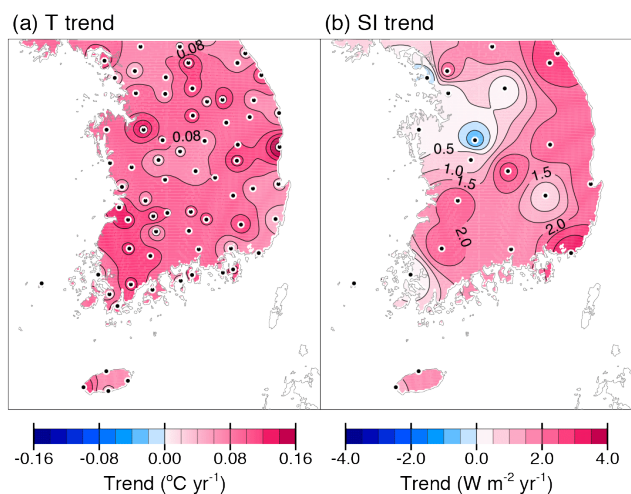


Figure 4. Spatial distributions of temporal linear trends of (a) daily average T and (b) daily average SI for the period 1999–2010 using data from 72 and 22 weather stations (black dots) of KMA, respectively.

Hemispheric land surface air temperature for the period 1979–2005 (IPCC, 2007). This highly increasing trend of temperature in South Korea is probably due to the urban heat island effect with rapid urbanization. The averaged temporal linear trend of insolation at 22 weather stations nationwide is about $+1.47 \text{ W m}^{-2} \text{ yr}^{-1}$ despite the decreasing phase of solar cycle during the 2000s. This is possibly caused by the reduction in particulate matter emissions due to enhanced environmental regulation in South Korea during the recent decade (KMOE, 2012).

Although O_3 and related meteorological variables such as temperature and insolation have recently increased in South Korea, the spatial patterns of their temporal trends do not show clear similarity. In addition, the spatial distribution of O_3 trends is rather inhomogeneous even on a metropolitan scale. For instance, Table 1 shows a wide range of O_3 trends among the SMA cities from -1.25 \% yr^{-1} at Gwacheon to $+2.82 \text{ \% yr}^{-1}$ at Seoul. The spatial inhomogeneity in O_3 trends and the trend differences among O_3 , temperature, and insolation imply that the long-term O_3 trends in South Korea are not only affected by changes in meteorological conditions but also influenced by changes in local precursor emissions or transport of O_3 and its precursors. The local effects of precursor emissions on the long-term changes in O_3 are further examined in Sect. 3.6.

3.2 Relationships between O_3 and meteorological variables

A multiple linear regression model is here adopted to explain relationships between $\text{O}_{3\text{8h}}$ and each of key meteorological variables such as T_{max} , SI, TD, PS, WS, and RH. To exclude day-to-day short-term fluctuations or white noises from

the original time series, $\text{KZ}_{29,3}$ was applied to each variable before the regression process and yielded baselines of each variable. As a result of the multiple linear regression, coefficients of determination (R^2) between baselines of $\text{O}_{3\text{8h}}$ and each meteorological variable, as well as adjusted R^2 for the multiple linear regression models, were calculated for 72 air quality monitoring sites distributed in 25 cities nationwide and summarized in Table 2. Combined meteorological effects on O_3 variations in each city are represented by adjusted R^2 , which adjusts for the number of predictors with consideration of the degrees of freedom. The nationwide average of adjusted R^2 is 0.51 and that of R^2 is 0.50 for SI, 0.29 for PS, 0.22 for T_{max} , 0.14 for TD, 0.05 for RH, and 0.03 for WS, respectively. In South Korea, SI, T_{max} , and TD generally show positive correlations with O_3 levels while PS is negatively correlated with O_3 variations. Since the short-term variability in each variable is excluded, the negative correlation between O_3 and PS is related to their seasonal cycle rather than continuously changing weather system of high and low. PS in South Korea, located on the continental east coast, is mostly affected by the cold continental high pressure air mass during the winter, when the O_3 concentrations are lowest. However, WS and RH show weak correlations with O_3 variations.

The spatial distributions of R^2 for T_{max} and SI, as well as the adjusted R^2 for the combined meteorological effects, are represented in Fig. 5. Both Fig. 5a and b show a common spatial pattern with high correlations at the inland and SMA cities and low correlations at the coastal cities. For instance, the average R^2 value with T_{max} for the coastal cities is only 0.07, which is much smaller than 0.36 for the SMA cities and 0.30 for the inland cities. Also, the average R^2 values with SI are 0.60 for the SMA cities and 0.58 for the inland cities, but 0.35 for the coastal cities. Despite the similar pattern between Fig. 5a and b, the R^2 values of SI are much higher than those of T_{max} because temperature affects net O_3 production rather indirectly compared to the direct influence of insolation on O_3 levels by photochemical production (Dawson et al., 2007, and references therein). The apparent R^2 differences among the three regions indicate that temporal variations of O_3 at the SMA and inland cities are much more sensitive to SI and T_{max} than those at the coastal cities. The low dependence of O_3 on T_{max} and SI at the coastal cities means that the photochemical reactions of precursors are less important for determining O_3 levels there compared to the SMA and inland cities.

The meteorological effects on O_3 at the inland, coastal, and SMA cities are also examined by daily minimum O_3 ($\text{O}_{3\text{min}}$). As represented in Fig. 6a and Table 3, the $\text{O}_{3\text{min}}$ is high near the coast, low at the inland cities, and lowest in the SMA. In the polluted urban area, the O_3 concentration reaches near-zero minima during the night since O_3 is reduced by NO_x titration, a nocturnal NO_y chemical process related to nitrate formation, and dry deposition in the absence of photochemical production. However, in the coastal region where the NO_x concentrations are low (Fig. 3b), the

Table 2. Coefficients of determination (R^2) between the baseline of daily maximum 8 h average O_3 (O_{38h}) and baselines of six meteorological variables (T_{max} , SI, TD, PS, WS, and RH) at 25 cities over South Korea for the period 1999–2010. Adjusted R^2 (Adj. R^2) between the baseline of O_{38h} and combined meteorological effects ($a_0 + \sum_i a_i MET_{BL}(t)_i$) are also represented. The cities are categorized into three groups: 10 coastal cities, 11 inland cities, and 4 cities in the SMA. Numbers in bold fonts indicate correlations significant at the 95 % level or higher.

	Cities	City code	Coefficients of determination (R^2)						Adj. R^2 MET _{BL}	
			T_{max}	SI	TD	PS	WS	RH		
Coastal region	Busan ¹	BS	0.147	0.366	0.139	0.222 ²	0.014	0.135	0.408	
	Changwon	CW	0.224	n/a	0.179	0.335 ²	0.001 ²	0.138	0.533	
	Gangneung	GN	0.013	0.480	0.000	0.072 ²	0.014	0.008 ²	0.449	
	Gunsan	GS	0.032	n/a	0.017	0.047 ²	0.002	0.003 ²	0.164	
	Jeju	JJ1	0.028 ²	0.080	0.069 ²	0.004	0.009	0.141 ²	0.337	
	Mokpo	MP	0.012	0.263	0.004	0.038 ²	0.047 ²	0.043 ²	0.427	
	Pohang	PH	0.034	0.404	0.014	0.102 ²	0.043 ²	0.003	0.398	
	Seosan	SS	0.059	0.495	0.021	0.135 ²	0.001	0.049 ²	0.506	
	Ulsan ¹	US	0.071	n/a	0.046	0.107 ²	0.035 ²	0.023	0.186	
	Yeosu	YS	0.093	n/a	0.061	0.140 ²	0.002 ²	0.024	0.251	
	Averages		0.071	0.348	0.055	0.120 ²	0.017	0.057	0.366	
Inland region	Andong	AD	0.269	0.544	0.128	0.379 ²	0.004	0.026 ²	0.628	
	Cheonan	CN	0.400	n/a	0.263	0.479 ²	0.003 ²	0.056 ²	0.674	
	Cheongju	CJ	0.387	0.666	0.219	0.443 ²	0.052	0.053 ²	0.674	
	Daegu ¹	DG	0.381	0.621	0.224	0.493 ²	0.002 ²	0.016	0.703	
	Daejeon ¹	DJ	0.312	0.721	0.160	0.408 ²	0.089	0.062 ²	0.724	
	Gumi	GM	0.244	n/a	0.116	0.361 ²	0.009 ²	0.038 ²	0.563	
	Gwangju ¹	GJ	0.274	0.502	0.159	0.315 ²	0.015	0.005 ²	0.570	
	Jecheon	JC	0.258	n/a	0.137	0.365 ²	0.012	0.108 ²	0.589	
	Jeonju	JJ2	0.134	0.434	0.060	0.179 ²	0.008 ²	0.038 ²	0.404	
	Jinju	JJ3	0.199	0.413	0.129	0.238 ²	0.000	0.012	0.396	
	Wonju	WJ	0.476	0.767	0.312	0.573 ²	0.069	0.018 ²	0.799	
		Averages		0.303	0.584	0.173	0.385 ²	0.024	0.039 ²	0.611
SMA	Ganghwa	GH	0.204	n/a	0.158	0.274 ²	0.190	0.025	0.389	
	Incheon ¹	IC	0.310	0.501	0.250	0.411 ²	0.019 ²	0.097	0.577	
	Seoul ¹	SU	0.419	0.580	0.318	0.531 ²	0.009 ²	0.045	0.693	
	Suwon	SW	0.525	0.703	0.422	0.640 ²	0.009	0.080	0.818	
		Averages		0.364	0.595	0.287	0.464 ²	0.057	0.062	0.619
Nationwide averages				0.220	0.502	0.144	0.292 ²	0.026	0.050 ²	0.514

¹ Major metropolitan cities in South Korea.

² Negative correlation.

n/a: not available observations of SI.

MET_{BL}: combined meteorological variables regressed on $[O_{3BL}] (a_0 + \sum_i a_i MET_{BL}(t)_i)$.

lower titration and nitrate formation at nighttime lead to the higher O_{3min} levels. In addition, transport of O_3 from the regional background could also keep high levels of O_3 during the night (Ghim and Chang, 2000). Frequency distributions of O_3 concentrations in previous studies suggested that O_3 levels at the coastal cities such as Gangneung, Jeju, Mokpo, Seosan, and Yeosu are affected by the background O_3 transport, unlike Seoul where the effect of local precursor emissions is dominant (Ghim and Chang, 2000; Ghim, 2000). Therefore, combined effects of the low NO_x levels and trans-

port of the regional background O_3 influence the high O_{3min} near the coast.

Compared to the spatial distribution of R^2 between baselines of O_{38h} and T_{max} or SI (Fig. 5a, b), O_{3min} distribution in Fig. 6a shows high O_{3min} at the coastal cities where the R^2 is low and low O_{3min} at the inland cities where the R^2 is high. These opposite patterns suggest that the meteorological effects on the O_3 production are negatively correlated with O_{3min} for the South Korean cities. The clear negative correlations are also shown in scatter plots (Fig. 6b, c). In both scatter plots, the three geographical groups of cities (blue for

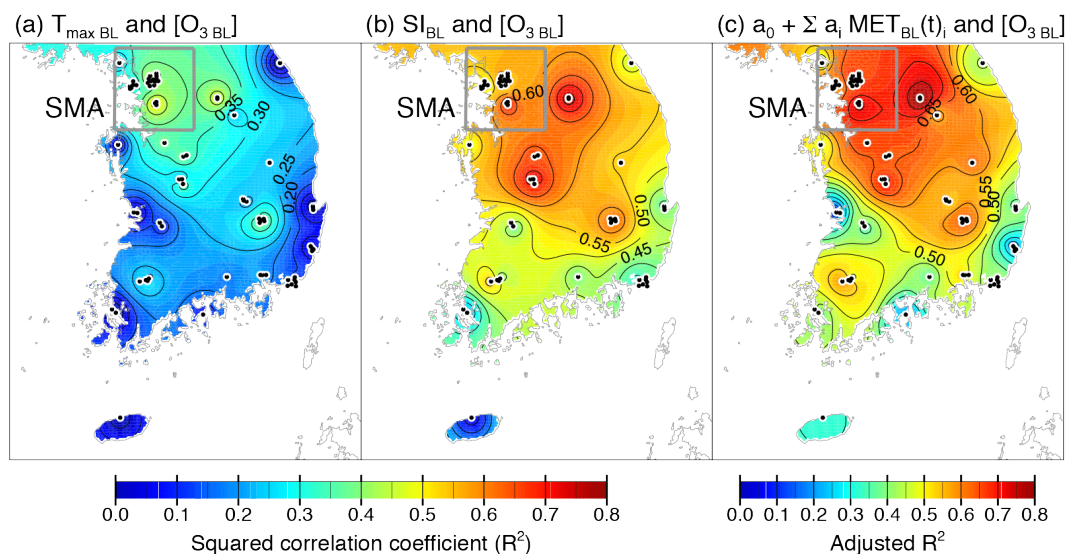


Figure 5. Spatial distributions of R^2 between baselines of O_3 ($[O_3, BL]$) and (a) daily maximum temperature ($T_{\max, BL}$) and (b) surface insolation (SI_{BL}). Black dots represent 72 air quality monitoring sites of NIER. (c) Spatial distribution of adjusted R^2 between $[O_3, BL]$ and combined meteorological effects ($a_0 + \sum_i a_i MET_{BL}(t)_i$).

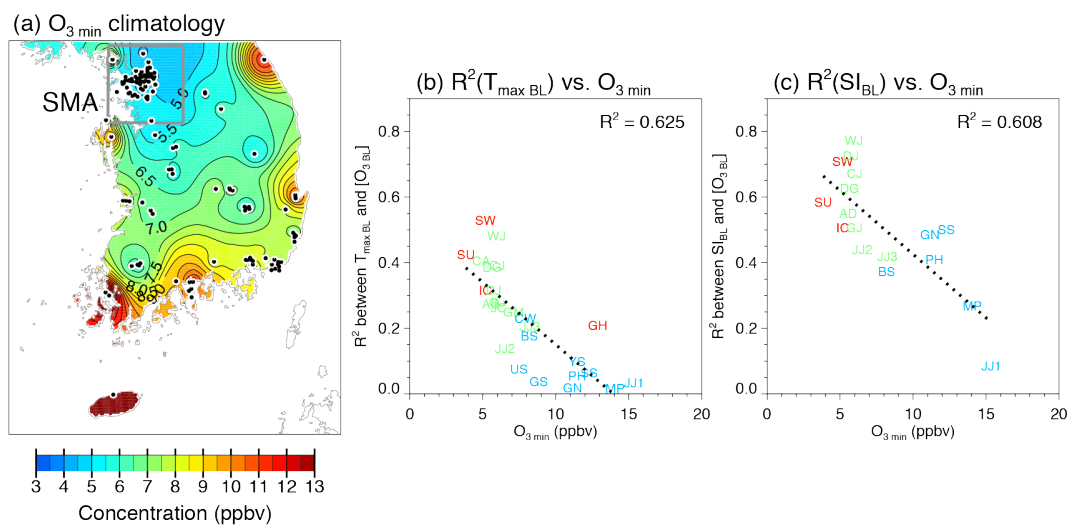


Figure 6. (a) Spatial distribution of 12 yr averaged concentrations of O_3, \min for the period 1999–2010 using data from 124 air quality monitoring sites (black dots) of NIER. (b) Scatter plot of R^2 between $[O_3, BL]$ and $T_{\max, BL}$ vs. O_3, \min at 25 cities. (c) Scatter plot of R^2 between $[O_3, BL]$ and SI_{BL} vs. O_3, \min at 17 cities. City codes in red, green, and blue indicate the SMA, inland, and coastal cities, respectively.

the coastal cities, green for the inland cities and red for SMA) are well separated. Several industrial or metropolitan cities in the coastal region such as Changwon (CW), Busan (BS), and Ulsan (US) have a relatively low O_3, \min compared to the other coastal cities. Larger NO_x emissions in these southeastern coastal cities (Fig. 3b) induce lower O_3, \min levels via NO_x titration and a nocturnal NO_y chemical process. Among the SMA cities, however, Ganghwa (GH) has much higher O_3, \min compared to other SMA cities. Ganghwa is a rural county located on the northwestern coast of the SMA. Therefore, both small NO_x emissions there and transport of regional back-

ground O_3 from the Yellow Sea affect the characteristics of O_3 in Ganghwa.

The different meteorological effects on O_3 between the coastal and inland regions are further examined with wind speed. Daily average WS data over South Korea are averaged for 12 yr. The 12 yr averaged WS is summarized in Table 3 and presented in a spatial map in Fig. 7a, which shows high wind speed in the coastal region and low wind speed in the inland region. Figure 7b and c show that the averaged wind speeds at 25 cities are positively correlated with O_3, \min and negatively correlated with the R^2 between O_3 and T_{\max} . In

Table 3. 12 yr averaged of daily minimum O₃ (O_{3min}) concentrations and daily average WS at 46 cities over South Korea for the period 1999–2010. The cities are categorized into three groups: 16 coastal cities, 14 inland cities, and 16 cities in the SMA.

Coastal region	City code	O _{3min} (ppbv)	WS (m s ⁻¹)	Inland region	City code	O _{3min} (ppbv)	WS (m s ⁻¹)	SMA	City code	O _{3min} (ppbv)	WS (m s ⁻¹)
Busan*	BS	8.2	3.38	Andong	AD	5.6	1.61	Ansan	–	5.7	n/a
Changwon	CW	7.9	2.01	Cheonan	CN	4.9	1.79	Anyang	–	3.9	n/a
Gangneung	GN	11.1	2.86	Cheongju	CJ	6.0	1.70	Bucheon	–	5.9	n/a
Gimhae	–	7.7	n/a	Daegu*	DG	5.6	2.31	Ganghwa	GH	12.9	1.84
Gunsan	GS	8.8	3.07	Daejeon*	DJ	5.7	1.96	Goyang	–	6.2	n/a
Gwangyang	–	12.9	n/a	Gimcheon	–	7.9	n/a	Gunpo	–	4.8	n/a
Jeju	JJI	15.4	3.31	Gumi	GM	7.1	1.53	Guri	–	4.4	n/a
Jinhae	–	13.3	n/a	Gwangju*	GJ	6.0	2.07	Gwacheon	–	4.8	n/a
Masan	–	8.6	n/a	Gyeongju	–	7.9	n/a	Gwangmyeong	–	5.6	n/a
Mokpo	MP	14.1	3.64	Iksan	–	6.4	n/a	Incheon*	IC	5.2	2.69
Pohang	PH	11.5	2.68	Jecheon	JC	6.1	1.51	Pyeongtaek	–	4.9	n/a
Seosan	SS	12.3	2.66	Jeonju	JJ2	6.5	2.02	Seongnam	–	5.8	n/a
Suncheon	–	9.4	1.16	Jinju	JJ3	8.2	1.37	Seoul*	SU	3.8	2.27
Ulsan*	US	7.5	2.12	Wonju	WJ	5.9	1.09	Siheung	–	6.6	n/a
Yeongam	–	13.7	n/a					Suwon	SW	5.2	1.86
Yeosu	YS	11.5	4.30					Uijeongbu	–	4.9	n/a
Coastal averages		10.9	2.84	Inland averages		6.4	1.72	SMA averages		5.6	2.17
Nationwide averages		7.7	2.26								

* Major metropolitan cities in South Korea.
n/a: not available observations of wind speed.

general, surface mixing and ventilation by high wind speeds reduce the near-surface precursors and thus decrease the photochemical production of O₃. Therefore the relationship between high wind speed and high O₃ levels in the coastal region is attributable to the transport of background O₃. However, the weaker wind speed induces a more effective photochemical reaction through the longer reaction time in stagnant conditions as well as more enhanced aerodynamic resistance to dry deposition (Jacob and Winner, 2009). Therefore, the effects of insolation and temperature on the O₃ productions become more important in the inland region where the wind speeds are lower.

3.3 Probability of O₃ exceedances related to temperature

Evaluating the probability of O₃ exceeding the air quality standard in a given range of temperature is useful to speculate about the potential sensitivity of O₃ concentrations to climate change (Lin et al., 2001; Jacob and Winner, 2009). Here we calculate the probabilities that O_{3,8h} exceeds the Korean air quality standard of 60 ppbv (KMOE, 2012) as a function of the daily maximum temperature (T_{\max}) for the coastal, inland, and SMA cities. Similar to the analyses in Lin et al. (2001) for the contiguous United States, Fig. 8 shows that the probabilities of O₃ exceedances increase with T_{\max} at the inland and SMA cities. For example, the probability of O₃ exceedances in the SMA is almost doubled by an increase

of about 4 °C in T_{\max} and reach 27 % at 30 °C. In the coastal region, however, the probability of O₃ exceedance increases up to 12–13 % with a T_{\max} change from 10 to 20 °C and does not increase significantly for T_{\max} above 20 °C. This is consistent with the spatial feature of the meteorological effects on O₃ levels, which are high at the inland and SMA cities and low at the coastal cities as described in the previous section. Therefore, the probability of high O₃ occurrence will be more sensitive to the future climate change at the inland and SMA cities than at the coastal cities. In the previous modeling study by Boo et al. (2006), T_{\max} over the Korean Peninsula is expected to rise by about 4–5 °C by the end of 21st century, due to global warming. This suggests considerable future increases in exceedances of the O₃ air quality standard over South Korea, except over coastal regions, in the absence of emission abatement measures.

3.4 Relative contributions of O₃ variations in different timescales

Surface O₃ variation can be decomposed into a short-term component ([O_{3,ST}]), seasonal component ([O_{3,SEASON}]), and long-term component ([O_{3,LT}]) by using the KZ filter as described in Sect. 2.2. We evaluated relative contributions of each component to the total variance of original time series. Overall, the relative contributions of [O_{3,LT}] in Fig. 9c are much smaller than those of [O_{3,ST}] in Fig. 9a and [O_{3,SEASON}]

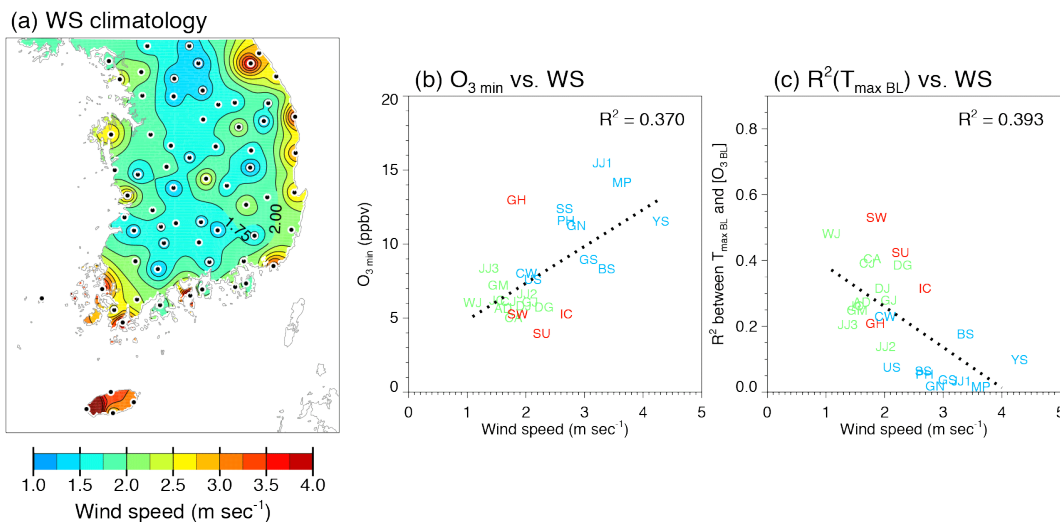


Figure 7. (a) Spatial distribution of 12 yr averaged daily average WS for the period 1999–2010 using data from 72 weather stations (black dots) of KMA. (b) Scatter plot of $O_{3\min}$ vs. WS at 25 cities. (c) Scatter plot of R^2 between $[O_{3BL}]$ and $T_{\max BL}$ vs. WS at 25 cities. City codes in red, green, and blue indicate the SMA, inland, and coastal cities, respectively.

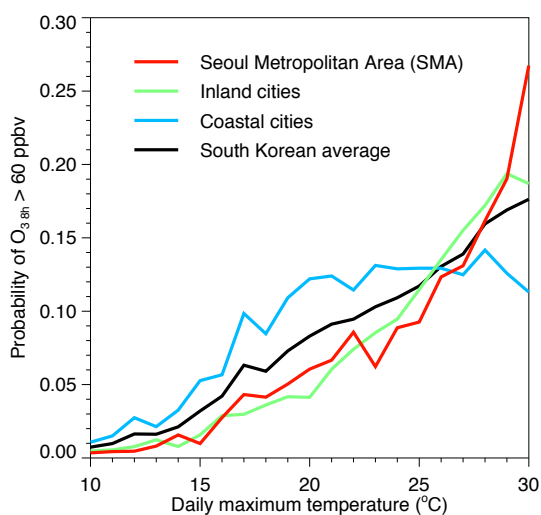


Figure 8. Probabilities of O_3 exceedances in the given range of daily maximum temperature (T_{\max}) that O_{38h} will exceed the air quality standard of South Korea (60 ppbv).

in b at all cities (Table 4). Therefore, sum of $[O_{3ST}]$ and $[O_{3SEASON}]$ account for the most of O_3 variations.

In Fig. 9a and b, the relative contributions of $[O_{3ST}]$ and $[O_{3SEASON}]$ show a strong negative relationship spatially. The relative contributions of $[O_{3ST}]$ are generally larger at the coastal cities (53.1 %) than at the inland cities (45.9 %), whereas the relative contributions of $[O_{3SEASON}]$ are smaller at the coastal cities (32.8 %) than at the inland cities (41.9 %).

Since $[O_{3ST}]$ is related to synoptic-scale weather fluctuations (Rao et al., 1995, 1997), the large relative contributions of $[O_{3ST}]$ at the coastal cities indicate the stronger effects of

the eastward-moving synoptic weather systems there. Interestingly, the highest value of the $[O_{3ST}]$ contribution appears at a northeastern coastal city, Gangneung. High and steep mountains on the west of Gangneung induce often warm, dry, and strong westerly winds, which is favorable to the clear sky and strong vertical mixing over the region. Since the westerly winds contain the precursors emitted from the SMA, the clear sky condition increases the O_3 levels during the daytime. In addition, the strong vertical mixing of high O_3 air from the free troposphere compensates the O_3 loss by titration during the nighttime. In the easterly winds, however, orographic lift often forms fog or clouds over the region and reduces the photochemical production of O_3 . Therefore, the combined effects of wind directions related to synoptic weather systems and topography increase the short-term variability of O_3 at Gangneung.

However, $[O_{3SEASON}]$ is driven mainly by the annual cycle of meteorological factors such as insolation or temperature. Therefore, the large relative contributions of $[O_{3SEASON}]$ at the inland cities are consistent with the higher impacts of temperature and insolation on O_3 there (Figs. 5, 9b). The highest and second-highest values of the $[O_{3SEASON}]$ contribution appear at Andong and Wonju, located in the inland basin. Since the basin topography often traps pollutants and induces large annual ranges of temperature, seasonal variability of O_3 at the two cities is larger than that of other inland cities.

$[O_{3LT}]$ explains less than 10 % of the total variances, but its relative contribution is considerable in the southwestern part of the Korean Peninsula as displayed in Fig. 9c. This is related to a relatively large long-term variability or trend in the region and is further discussed in Sect. 3.6.

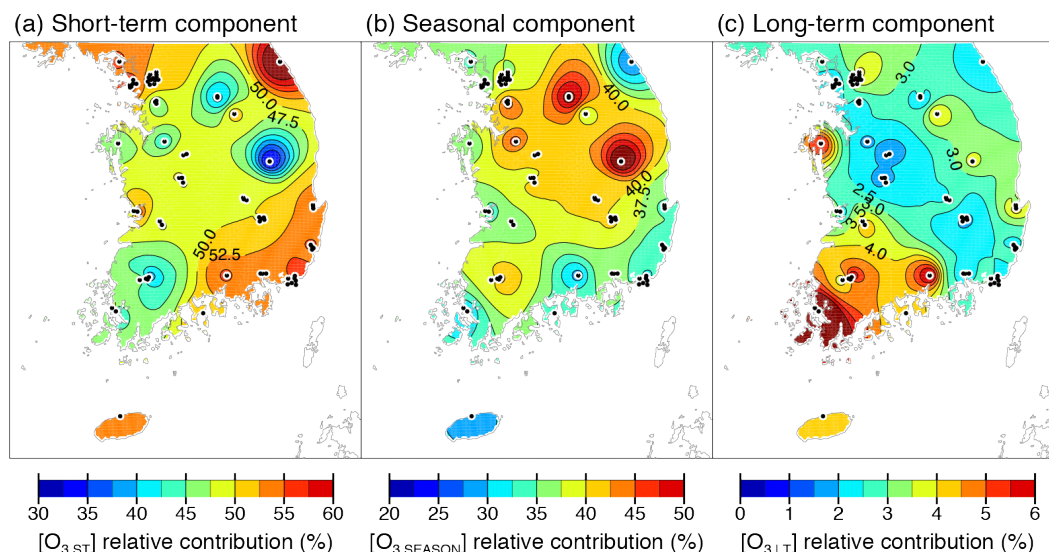


Figure 9. Spatial distributions of relative contributions of the (a) short-term component ($[O_{3ST}]$), (b) seasonal component ($[O_{3SEASON}]$), and (c) long-term component ($[O_{3LT}]$) to the total variance of original time series ($[O_3]$) using data from 72 air quality monitoring sites (black dots) of NIER. Note that the color scales are all different.

Table 4. Relative contributions (%) of short-term components ($[O_{3ST}]$), seasonal components ($[O_{3SEASON}]$), and long-term components ($[O_{3LT}]$) to total variance of log-transformed daily maximum 8 h average O_3 ($[O_3]$) at 25 cities over South Korea for the period 1999–2010. The cities are categorized into three groups: 10 coastal cities, 11 inland cities, and 4 cities in the SMA.

Coastal region	City code	Relative contributions (%)			Inland region	City code	Relative contributions (%)			SMA	City code	Relative contributions (%)		
		$[O_{3ST}]$	$[O_{3SEASON}]$	$[O_{3LT}]$			$[O_{3ST}]$	$[O_{3SEASON}]$	$[O_{3LT}]$			$[O_{3ST}]$	$[O_{3SEASON}]$	$[O_{3LT}]$
Busan*	BS	56.1	32.6	2.5	Andong	AD	32.7	53.2	3.6	Ganghwa	GH	56.2	33.1	3.2
Changwon	CW	53.6	36.2	2.0	Cheonan	CN	41.5	46.5	1.8	Incheon*	IC	58.7	32.7	1.5
Gangneung	GN	62.5	29.1	2.0	Cheongju	CJ	48.3	41.7	1.3	Seoul*	SU	51.8	38.2	3.8
Gunsan	GS	52.3	34.2	2.7	Daegu*	DG	50.4	41.3	1.6	Suwon	SW	42.0	49.4	1.8
Jeju	JJI	53.8	29.2	4.3	Daejeon*	DJ	49.2	40.5	1.5					
Mokpo	MP	46.1	30.9	8.5	Gumi	GM	48.2	42.0	2.7					
Pohang	PH	53.9	34.4	4.1	Gwangju*	GJ	41.5	41.3	4.8					
Seosan	SS	45.1	35.6	5.3	Jecheon	JC	50.8	38.6	4.0					
Ulsan*	US	55.5	32.1	2.5	Jeonju	JJ2	47.4	36.1	4.2					
Yeosu	YS	52.2	34.1	4.3	Jinju	JJ3	55.5	29.2	6.2					
					Wonju	WJ	39.5	50.8	2.3					
Coastal averages		53.1	32.8	3.8	Inland averages		45.9	41.9	3.1	SMA averages		52.2	38.3	2.6
Nationwide averages		49.8	37.7	3.3										

* Major metropolitan cities in South Korea

3.5 Short-term variation of O_3 related to wind direction

The short-term components of O_3 ($[O_{3ST}]$) account for a large fraction of total O_3 variation over South Korea. In Table 4, relative contributions of $[O_{3ST}]$ range from 32.7 to 62.5% and have a nationwide average of 49.8%. Therefore, it is no wonder that high O_3 episodes are mostly determined by day-to-day fluctuation of $[O_{3ST}]$. One considerable factor influencing the short-term variation of O_3 is wind. Shin et al. (2012) displayed $[O_{3ST}]$ on the wind speed-direction domain and showed that the effects of episodic long-range transport and local precursor emission on the ambient O_3 concentrations could be qualitatively separated from $[O_{3ST}]$.

We here further investigate the transport effect on the short-term variations of O_3 and the frequency of high O_3 episodes using $\exp[O_{3ST}]$ and WDs. As described in Sect. 2.2, $\exp[O_{3ST}]$ is a ratio of the raw O_{38h} concentration to its baseline concentration in ppbv ($\exp[O_{3BL}]$). Thus, the O_{38h} concentration is higher than the baseline O_{38h} concentration when $\exp[O_{3ST}] > 1$. We classified every single value of $\exp[O_{3ST}]$ with the eight cardinal WDs during the months of frequent high O_3 events (May–October) at all available monitoring sites within each city. The probabilities of $\exp[O_{3ST}] > 1$ for each WD were compared with the probabilities of exceeding the South Korean air quality standard of 60 ppbv for O_{38h} .

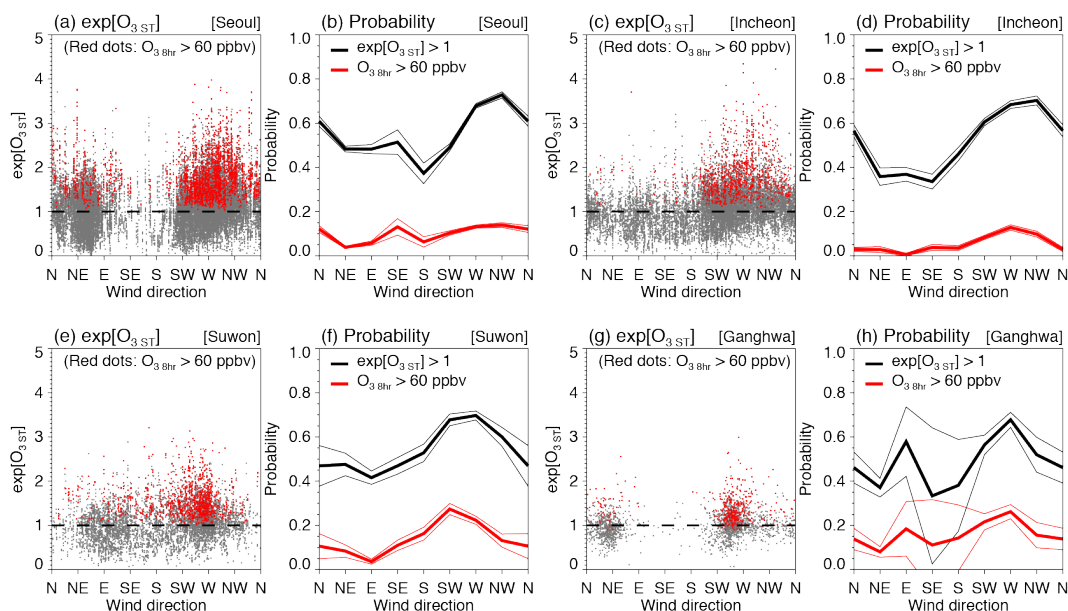


Figure 10. Relationships between WD and exponentials of short-term components ($\exp[\text{O}_3\text{ST}]$) during the months of frequent high O_3 events (May–October) at Seoul (a–b), Incheon (c–d), Suwon (e–f), and Ganghwa (g–h) in the SMA are represented in scatter plots of $\exp[\text{O}_3\text{ST}]$ vs. WD (a, c, e, and g) and probabilities of O_3 exceedances in each WD (b, d, f, and h). Red dots in scatter plots denote high O_3 episodes in which the daily maximum 8 h average O_3 ($\text{O}_{3\text{8hr}}$) will exceed the air quality standard of South Korea (60 ppbv). Dashed lines in scatter plots denote the reference of $\exp[\text{O}_3\text{ST}] = 1$. Probabilities of $\exp[\text{O}_3\text{ST}] > 1$ and $\text{O}_{3\text{8hr}} > 60$ ppbv in each WD are represented as black thick lines and red thick lines, respectively. The black and red thin lines represent the 95 % of confidence intervals for each probability. We used O_3 data from 12 sites in Seoul, 6 sites in Incheon, 3 sites in Suwon, and 1 site in Ganghwa.

Figure 10 shows $\exp[\text{O}_3\text{ST}]$ in the SMA cities (Seoul, Incheon, Suwon, and Ganghwa) with probabilities of $\exp[\text{O}_3\text{ST}] > 1$ and $\text{O}_{3\text{8hr}} > 60$ ppbv for each WD. In Seoul, high O_3 episodes occur mostly during northwesterly winds although westerly and northeasterly winds predominate during the months of frequent high O_3 events (Fig. 10a, b). The high probability of high O_3 in northwesterly winds in Seoul is similar to those in other neighboring cities in the SMA, where the high probability also occurs during northwesterly winds in Incheon located in the west of Seoul (Fig. 10c, d), and during westerly winds in Suwon in the south of Seoul (Fig. 10e, f), and in Ganghwa in the northwest of Seoul (Fig. 10g, h).

The sea–mountain breeze can explain the prevalence of high O_3 episodes under westerly or northwesterly winds in the SMA. In the western coast of the SMA, there are many thermoelectric power plants (see triangles in Figs. 11 and 12) and industrial complexes, which directly emit a large amount of O_3 precursors. Heavy inland and maritime transportation in those regions is also an important source of NO_x and hydrocarbon emissions. Since the SMA is surrounded by the Yellow Sea in the west and a mountainous region in the east (see Fig. 1), the westerly sea breeze is well developed under O_3 -conductive meteorological conditions such as high temperature and strong insolation with low wind speed (Ghim and Chang, 2000; Ghim et al., 2001). In addition, locally

emitted precursors and transported background O_3 from the west are trapped in the SMA due to the westerly sea breeze and the mountainous terrain in the east of the SMA. Therefore, the O_3 concentrations in the SMA increase in such O_3 -conductive meteorological conditions with near-westerly winds.

Another factor to increase the high O_3 probabilities in the near-westerly winds is long-range transport of O_3 and its precursors from China. For example, Ghim et al. (2001) reported some high O_3 cases in the SMA, which result from the transport of O_3 -rich air with strong westerly wind at dawn under overcast conditions. Oh et al. (2010) also showed that the elevated layer of high O_3 concentration over the SMA is associated with the long-range transport of O_3 from eastern China. As the mixing layer thickens over the SMA, the O_3 concentration can increase by up to 25 % via the vertical down-mixing process (Oh et al., 2010). Recently, Kim et al. (2012) showed that westerly winds also transport O_3 precursors such as NO_2 and carbon monoxide (CO) from China to South Korea.

Interestingly, the high O_3 probability in Ganghwa (Fig. 10g, h) shows a bimodal distribution with another peak in easterly wind. Considering that Ganghwa is a rural county on the northwestern coast of the SMA, the double peak of high O_3 probability in easterly and westerly winds shows the effects of both local- and long-range transport.

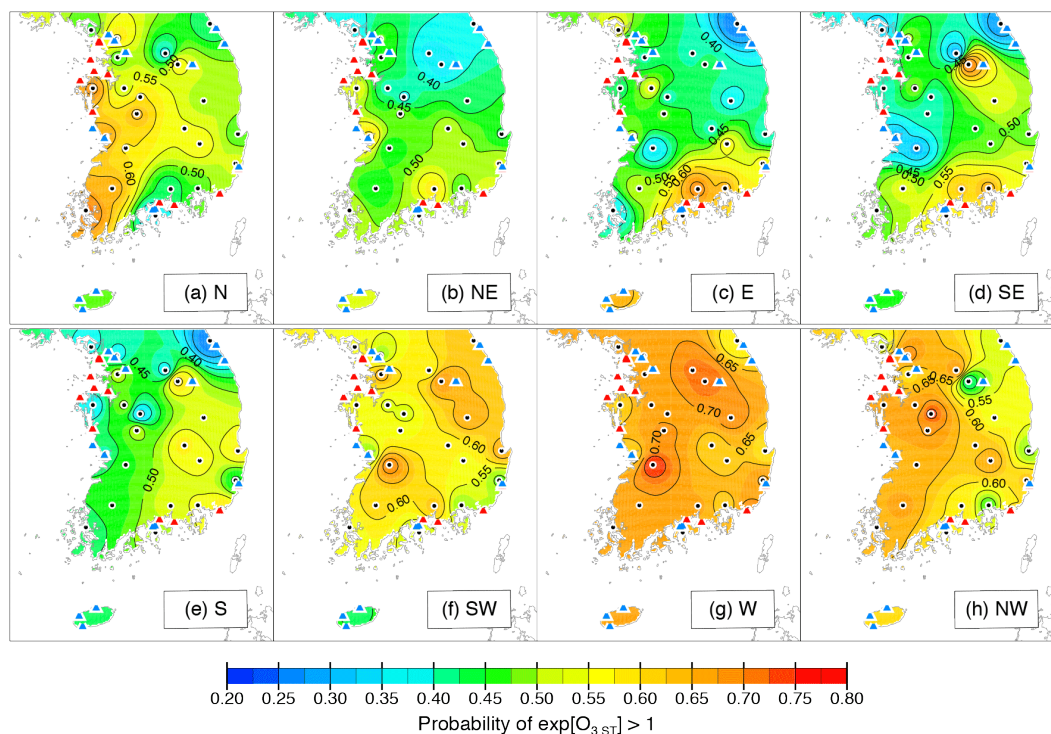


Figure 11. Spatial distributions of probabilities that exponentials of the short-term components will exceed 1 ($\exp[\text{O}_3_{\text{ST}}] > 1$) for each WD: (a) northerly (N), (b) northeasterly (NE), (c) easterly (E), (d) southeasterly (SE), (e) southerly (S), (f) southwesterly (SW), (g) westerly (W), and (h) northwesterly (NW), respectively. Black dots denote 25 weather stations of KMA and triangles denote 26 major thermoelectric power plants in South Korea (blue triangle < 1000 MW, red triangles ≥ 1000 MW).

We extended the above $\exp[\text{O}_3_{\text{ST}}]$ and WD analysis to 25 cities in South Korea. The nationwide view of the high O_3 probabilities is represented by the probabilities of $\exp[\text{O}_3_{\text{ST}}] > 1$ and $\text{O}_3_{8\text{h}} > 60$ ppbv by each wind direction during the months of frequent high O_3 events (May–October). Figures 11 and 12 show spatial maps of the probabilities of $\exp[\text{O}_3_{\text{ST}}] > 1$ and $\text{O}_3_{8\text{h}} > 60$ ppbv, respectively. As indicators of major precursor emission point sources, we marked 26 of major thermoelectric power plants with triangles on the map. In general, most of the thermoelectric power plants are located in the western coast of the SMA and southeastern coastal region of the Korean Peninsula. Thermoelectric power plants are important sources of NO_x in South Korea, accounting for 13 % (0.14 Mt) of total NO_x emissions nationwide (KMOE, 2013). Considering that industrial complexes over South Korea are mostly concentrated near the power plants, the area with triangles in Figs. 11 and 12 represents major sources of O_3 precursors.

In Figs. 11 and 12, both probabilities of $\exp[\text{O}_3_{\text{ST}}] > 1$ and $\text{O}_3_{8\text{h}} > 60$ ppbv are generally high on a national scale during the near-westerly wind conditions (Figs. 11f–h, 12f–h). The prevailing westerly wind of the synoptic-scale flow transports O_3 and its precursors from China to South Korea and thus increases the probability of high O_3 episodes as well as high O_3 concentrations. However, on a local scale,

the high-probability regions of high O_3 correspond to those downwind of the thermoelectric power plants. For example, the high probabilities of high O_3 in the southeastern part of South Korea, downwind of power plants along the southeastern coast, also appear even during the easterly or southerly winds (Figs. 11c–e, 12c–e). Therefore, the spatial features of the high O_3 probabilities for each wind direction could be associated with both the local effect of precursor emissions and long-range transport from the continent.

3.6 Long-term variation of O_3 and local precursor emissions

The temporal linear trend of baseline ($[\text{O}_3_{\text{BL}}]$) is almost the same as that of the original time series since the short-term component ($[\text{O}_3_{\text{ST}}]$) is nearly detrended. Therefore, the O_3 trend can be represented as a sum of the seasonal component ($[\text{O}_3_{\text{SEASON}}]$) and long-term component ($[\text{O}_3_{\text{LT}}]$) trends. The spatial trend distributions of $[\text{O}_3_{\text{BL}}]$ and its two separated components of seasonal and long-term components are shown in Fig. 13. It is noted that the period used in Fig. 13 is shorter than the total period of original data because of truncation effect in the KZ filter process. The long-term component obtained by the KZ filter of $\text{KZ}_{365,3}$ loses 546 days at the beginning and end of the original time series.

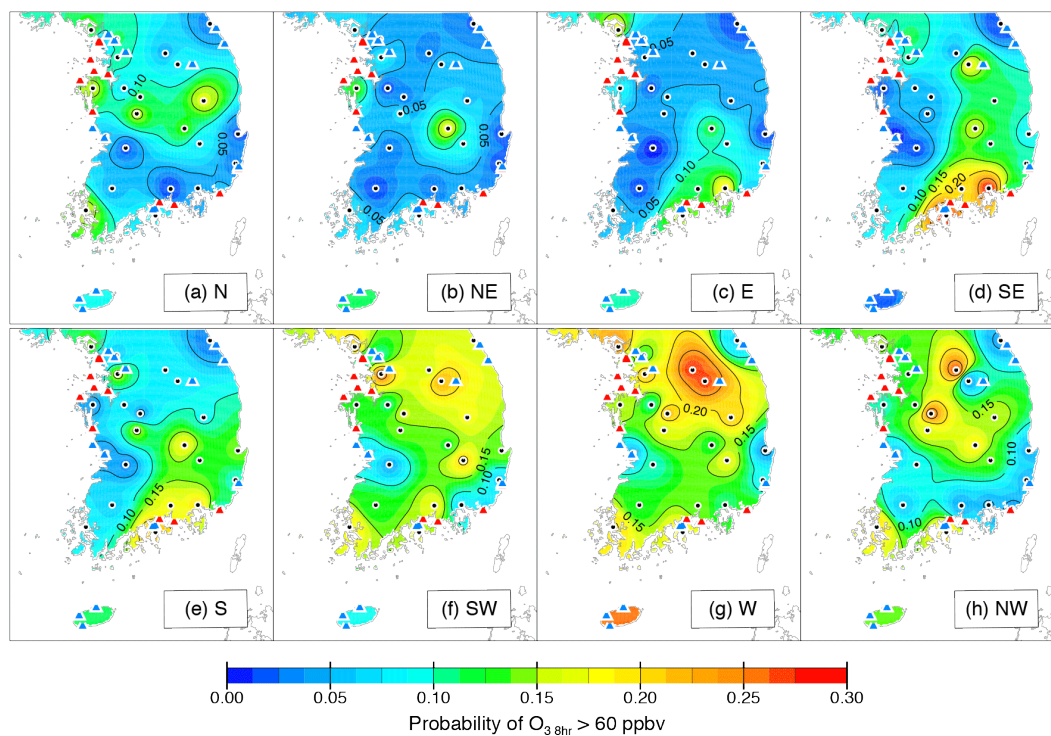


Figure 12. Spatial distributions of probabilities that the daily maximum 8 h average O_3 ($O_{3,8h}$) will exceed the air quality standard of South Korea (60 ppbv) for each WD: (a) N, (b) NE, (c) E, (d) SE, (e) S, (f) SW, (g) W, and (h) NW, respectively. Black dots denote 25 weather stations of KMA and triangles denote 26 major thermoelectric power plants in South Korea (blue triangle < 1000 MW, red triangles \geq 1000 MW).

The increasing trends of O_3 are generally high in the SMA and southwestern region and low in the southeastern coastal region of the Korean Peninsula (Fig. 13a). This spatial inhomogeneity of the O_3 trends over South Korea is mainly caused by the long-term component trends (Fig. 13c) rather than the seasonal component trend (Fig. 13b). Therefore, the large spatial variability in local precursor emissions induced the spatial inhomogeneity of O_3 trends in South Korea. However, a relatively homogeneous distribution of the seasonal component trends implies that meteorological influences on the long-term changes in O_3 have little regional dependence nationwide.

Since the spatially inhomogeneous O_3 trends are related to the local precursor emissions, we also tried to investigate their relationship with NO_2 measurement data. To detect temporally synchronous and spatially coupled patterns between the long-term variations of O_3 and NO_2 , we applied the SVD to $[O_{3,LT}]$ and the long-term component of NO_2 ($[NO_{2,LT}]$). $[NO_{2,LT}]$ was simply obtained by applying the KZ filter of $KZ_{365,3}$ to the log-transformed NO_2 time series. The SVD is usually applied to two combined space–time data fields, based on the computation of a temporal cross-covariance matrix between two data fields. The SVD identifies coupled spatial patterns and their temporal variations, with each pair of spatial patterns explaining a fraction of the

squared covariance between the two space–time data sets. The squared covariance fraction (SCF) is largest in the first pair (mode) of the patterns, and each succeeding mode has a maximum SCF that is unexplained by the previous modes.

The first three leading SVD modes (singular vectors) of the coupled O_3 and NO_2 long-term components account for the SCF with 94.6% of the total, of which the first, second, and third modes are 63.7, 23.6, and 7.3%, respectively. Figure 14 displays the expansion coefficients (coupled spatial patterns) and their time series of the first mode along with a spatial map of the $[NO_{2,LT}]$ trends. The dominant first mode of the O_3 and NO_2 long-term components (Fig. 14a, b) is very similar to the spatial distributions of $[O_{3,LT}]$ trends (Fig. 13c) and $[NO_{2,LT}]$ trends (Fig. 14c), respectively. In Fig. 14d, the strong coherence in the time series is observed between the first modes of the $[O_{3,LT}]$ and $[NO_{2,LT}]$ with a correlation coefficient of 0.98. The results of SVD analyses suggest that the long-term variations of O_3 and NO_2 in South Korea have similar temporal evolutions with different spatial patterns.

The differences in spatial patterns of $[O_{3,LT}]$ and $[NO_{2,LT}]$ as shown in Fig. 14a and b require to be further investigated. Since the VOC emissions from industry, transportation, and the solvent usage in construction are large in South Korea (KMOE, 2013), further analyses of VOC measurements

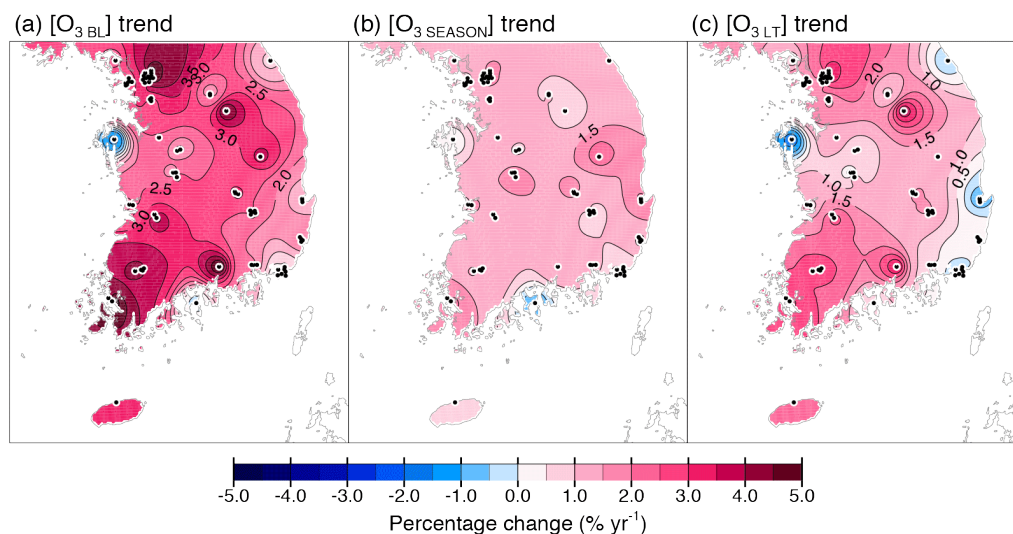


Figure 13. Spatial distributions of temporal linear trends of the (a) baseline ($[O_3]_{BL}$), (b) seasonal component ($[O_3]_{SEASON}$), and (c) long-term component ($[O_3]_{LT}$) for the period 2000–2009 using data from 72 air quality monitoring sites of NIER.

are needed. On top of that, especially in South Korea, biogenic precursor emissions are also potentially important for the analysis due to dense urban vegetation in and around metropolitan areas. Therefore, there remains the limitation of our current data analysis due to the lack of both VOC emission data and observations of atmospheric concentrations of VOCs in South Korea.

4 Conclusions

This study has investigated various spatiotemporal features and the interrelationship of surface O_3 and related meteorological variables over South Korea based on ground measurements for the period 1999–2010. A general overview of surface O_3 in terms of spatial distributions and its temporal trend is provided based on its decomposed components by the KZ filter.

In South Korea, the O_3 concentrations are low at the inland and SMA cities due to the NO_x titration by anthropogenic emissions and high at the coastal cities possibly due to the dynamic effects of the sea breeze. The averaged O_3 levels in South Korea have increased for the period 1999–2010 with an averaged temporal linear trend of $+0.26 \text{ ppbv yr}^{-1}$ ($+1.15 \% \text{ yr}^{-1}$). The recent increase of the O_3 levels in East Asia may result from the recent increase of anthropogenic precursor emissions and the long-term variations in meteorological effects.

We applied a linear regression model to investigate the relationships between O_3 and meteorological variables such as temperature, insolation, dew-point temperature, sea-level pressure, wind speed, and relative humidity. Spatial distribution of the R^2 values shows high meteorological influences in the SMA and inland regions and low meteorological in-

fluences in the coastal region. The high meteorological influences in the SMA and inland regions are related to effective photochemical activity, which results from large local precursor emissions and stagnant conditions with low wind speeds. However, the low meteorological influences in the coastal region are related to large transport effects of the background O_3 and ventilation and dry deposition with high wind speeds.

In the SMA and inland region, the high O_3 probability ($O_{38h} > 60 \text{ ppbv}$) increases with the daily maximum temperature rise. Specifically in the SMA, the most populated area in South Korea, the probability of the O_3 exceedances is almost doubled by a 4°C increase in daily maximum temperature and reached 27% at 30°C . It is noted that the variations in O_3 exceedance probabilities according to the maximum temperature show an approximate logarithmic increase in the SMA and inland regions. It thus implies that these regions will experience more frequent high O_3 events in future climate conditions with the increasing global temperature.

The O_3 time series observed at each monitoring site can be decomposed into the short-term, seasonal, and long-term components by the KZ filter. Relative contributions of each separated component show that the short-term and seasonal variations account for most of the O_3 variability. Relative contributions of the short-term component are large at the coastal cities due to influence of the background O_3 transport. In contrast, those of the seasonal component are large at the inland cities due to the high meteorological influences on the O_3 variations.

The transport effects on the short-term component are shown in the probability distributions of both high short-term component values and O_3 exceedances for each wind direction. During the months of frequent high O_3 events (May–October) in South Korea, the probabilities of both high

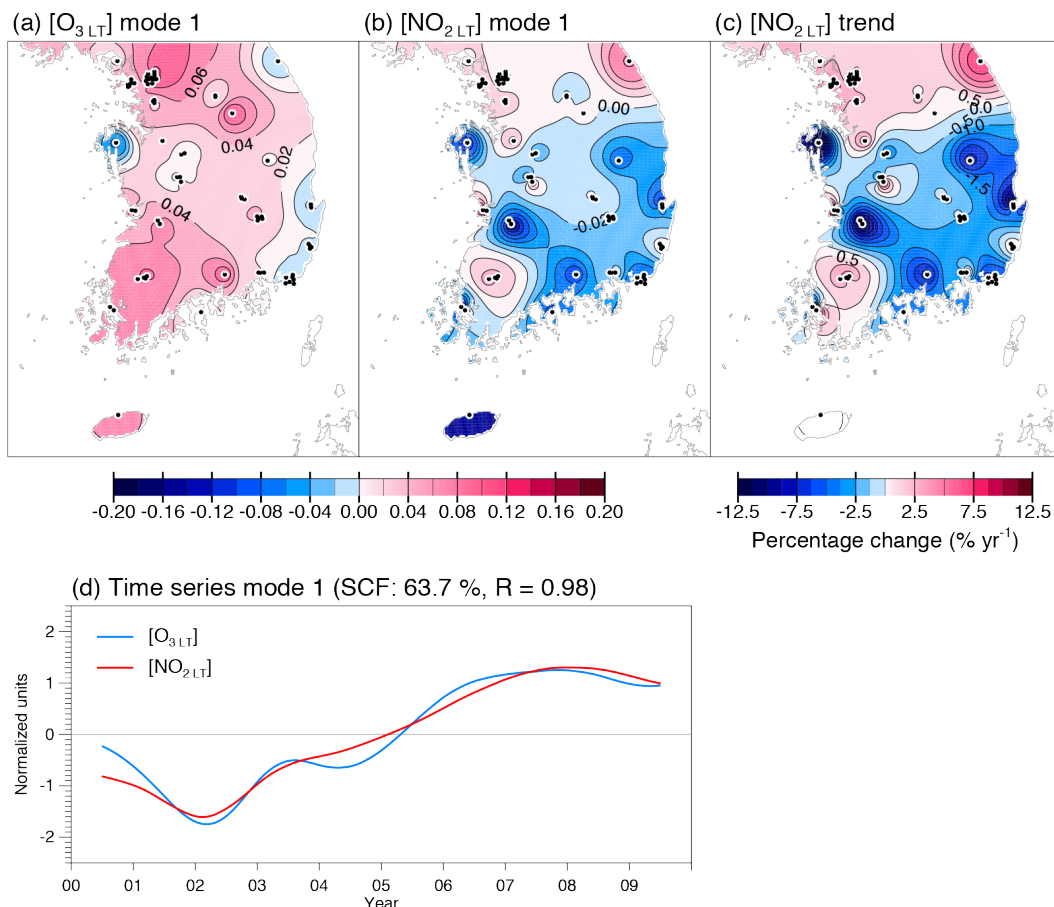


Figure 14. The first leading mode of SVD between the long-term components of (a) daily maximum 8 h average O_3 ($[O_{3LT}]$) and (b) daily average NO_2 ($[NO_{2LT}]$) for the period 2000–2009. (c) Spatial distribution of temporal linear trends of $[NO_{2LT}]$. (d) Time series of the SVD expansion coefficient associated with $[O_{3LT}]$ mode (blue line) and $[NO_{2LT}]$ mode (red line).

short-term component O_3 and O_3 exceedances are higher in the near-westerly wind condition rather than in other wind directions. For the short-term timescale, the eastward long-range transport of O_3 and precursors from China can cause the nationwide high probabilities of O_3 exceedances in the near-westerly wind condition. However, the high probabilities of extreme O_3 events in downwind regions of the thermoelectric power plants and industrial complexes are related to local transport of O_3 precursors, which apparently enhances the O_3 levels.

The distribution of O_3 trends in South Korea is spatially inhomogeneous. Although the relative contributions of the long-term components are much smaller than those of the other two components. Such a spatially inhomogeneous distribution of the O_3 trend is mainly caused by the long-term component O_3 trends rather than the seasonal component O_3 trend related to the long-term change of meteorological conditions, which is because the long-term change of the local precursor emission has a localized effect on the long-term O_3 change. The SVD between O_3 and NO_2 shows that the long-term variations of O_3 and NO_2 in South Korea have similar

temporal evolutions with different spatial patterns. The results of SVD analyses clearly demonstrate the influences of local precursor emissions on the long-term changes in O_3 . However, the precise interpretation of the large spatially inhomogeneous distribution in the long-term component O_3 trend is limited due to the lack of VOC measurements data.

The KZ filter is a useful diagnostic tool to reveal the spatiotemporal features of O_3 and its relationship with meteorological variables. General features revealed by the KZ filter analysis will provide a better understanding of spatial and temporal variations of surface O_3 as well as possible influences of local emissions, transport, and climate change on O_3 levels in South Korea. Our analyses can also be helpful as a reference for the evaluation of chemistry transport models and furthermore for establishing appropriate O_3 control policies.

The Supplement related to this article is available online at [doi:10.5194/acp-14-6395-2014-supplement](https://doi.org/10.5194/acp-14-6395-2014-supplement).

Acknowledgements. This study has been funded by the Green City Technology Flagship Program of the Korea Institute of Science and Technology. D. Youn was supported by Chungbuk National University. This work was done as H. Lee's private venture and not in the author's capacity as an employee of the Jet Propulsion Laboratory, California Institute of Technology. The authors also appreciate constructive comments from two anonymous referees.

Edited by: K. Schaefer

References

- Akimoto, H.: Global air quality and pollution, *Science*, 302, 1716–1719, doi:10.1126/science.1092666, 2003.
- Bell, M. L., Goldberg, R., Hogrefe, C., Kinney, P. L., Knowlton, K., Lynn, B., Rosenthal, J., Rosenzweig, C., and Patz, J. A.: Climate change, ambient ozone, and health in 50 US cities, *Clim. Change*, 82, 61–76, doi:10.1007/s10584-006-9166-7, 2007.
- Bernard, S. M., Samet, J. M., Grambsch, A., Ebi, K. L., and Romieu, I.: The potential impacts of climate variability and change on air pollution-related health effects in the United States, *Environ. Health Persp.*, 109, 199–209, 2001.
- Boo, K.-O., Kwon, W.-T., and Baek, H.-J.: Change of extreme events of temperature and precipitation over Korea using regional projection of future climate change, *Geophys. Res. Lett.*, 33, L01701, doi:10.1029/2005GL023378, 2006.
- Camalier, L., Cox, W., and Dolwick, P.: The effects of meteorology on ozone in urban areas and their use in assessing ozone trends, *Atmos. Environ.*, 41, 7127–7137, doi:10.1016/j.atmosenv.2007.04.061, 2007.
- Carmichael, G. R., Uno, I., Phadnis, M. J., Zhang, Y., and Sunwoo, Y.: Tropospheric ozone production and transport in the springtime in East Asia, *J. Geophys. Res.*, 103, 10649–10671, doi:10.1029/97JD03740, 1998.
- Chatani, S. and Sudo, K.: Influences of the variation in inflow to East Asia on surface ozone over Japan during 1996–2005, *Atmos. Chem. Phys.*, 11, 8745–8758, doi:10.5194/acp-11-8745-2011, 2011.
- Dawson, J. P., Adams, P. J., and Pandis, S. N.: Sensitivity of ozone to summertime climate in the eastern USA: A modeling case study, *Atmos. Environ.*, 41, 1494–1511, doi:10.1016/j.atmosenv.2006.10.033, 2007.
- Dibb, J. E., Talbot, R. W., Scheuer, E., Seid, G., DeBell, L., Lefer, B., and Ridley, B.: Stratospheric influence on the northern North American free troposphere during TOPSE: ^7Be as a stratospheric tracer, *J. Geophys. Res.*, 108, 8363, doi:10.1029/2001JD001347, 2003.
- Diem, J. E.: A critical examination of ozone mapping from a spatial-scale perspective, *Environ. Pollut.*, 125, 369–383, doi:10.1016/S0269-7491(03)00110-6, 2003.
- Ding, A. J., Wang, T., Thouret, V., Cammas, J.-P., and Nédélec, P.: Tropospheric ozone climatology over Beijing: analysis of aircraft data from the MOZAIC program, *Atmos. Chem. Phys.*, 8, 1–13, doi:10.5194/acp-8-1-2008, 2008.
- Eskridge, R. E., Ku, J. Y., Rao, S. T., Porter, P. S., and Zurbenko, I. G.: Separating different scales of motion in time scales of motion in time series of meteorological variables, *B. Am. Meteorol. Soc.*, 78, 1473–1483, doi:10.1175/1520-0477(1997)078<1473:SDSOMI>2.0.CO;2, 1997.
- Flaum, J. B., Rao, S. T., and Zurbenko, I. G.: Moderating the influence of meteorological conditions on ambient ozone concentrations, *J. Air Waste Manage.*, 46, 35–46, doi:10.1080/10473289.1996.10467439, 1996.
- Gardner, M. W. and Dorling, S. R.: Meteorologically adjusted trends in UK daily maximum surface ozone concentrations, *Atmos. Environ.*, 34, 171–176, doi:10.1016/S1352-2310(99)00315-5, 2000.
- Ghim, Y. S.: Trends and factors of ozone concentration variations in Korea, *Journal of Korean Society for Atmospheric Environment*, 16, 607–623, 2000 (in Korean).
- Ghim, Y. S. and Chang, Y. S.: Characteristics of ground-level ozone distribution in Korea for the period of 1990–1995, *J. Geophys. Res.*, 105, 8877–8890, doi:10.1029/1999JD901179, 2000.
- Ghim, Y. S., Oh, H. S., and Chang, Y. S.: Meteorological effects on the evolution of high ozone episodes in the Greater Seoul Area, *J. Air Waste Manage.*, 51, 185–202, doi:10.1080/10473289.2001.10464269, 2001.
- Guicherit, R. and Roemer, M.: Tropospheric ozone trends, *Chemosphere-Global Change Science*, 2, 167–183, 2000.
- Ibarra-Berastegi, G., Madariaga, I., Elías, A., Agirre, E., and Uria, J.: Long-term changes of ozone and traffic in Bilbao, *Atmos. Environ.*, 35, 5581–5592, doi:10.1016/S1352-2310(01)00210-2, 2001.
- IPCC (Intergovernmental Panel on Climate Change): Climate Change 2007: The Physical Scientific Basis: Contribution of Working Group I to the Fourth Assessment Report of the Intergovernmental Panel on Climate Change, edited by: Solomon, S., Qin, D., Manning, M., Chen, Z., Marquis, M., Averyt, K. B., Tignor, M., and Miller, H. L., Cambridge University Press, Cambridge, United Kingdom and New York, NY, USA, 2007.
- Jacob, D. J. and Winner, D. A.: Effect of climate change on air quality, *Atmos. Environ.*, 43, 51–63, doi:10.1016/j.atmosenv.2008.09.051, 2009.
- Jacob, D. J., Logan, J. A., and Murti, P. P.: Effect of rising Asian emissions on surface ozone in the United States, *Geophys. Res. Lett.*, 26, 2175–2178, doi:10.1029/1999GL900450, 1999.
- Jaffe, D. A., Parrish, D., Goldstein, A., Price, H., and Harris, J.: Increasing background ozone during spring on the west coast of North America, *J. Geophys. Res.*, 30, 1613, doi:10.1029/2003GL017024, 2003.
- Jin, L., Lee, S.-H., Shin, H.-J., and Kim, Y. P.: A study on the ozone control strategy using the OZIPR in the Seoul Metropolitan Area, *Asian J. Atmos. Environ.*, 6, 111–117, doi:10.5572/ajae.2012.6.2.111, 2012.
- Kim, J. Y., Kim, S.-W., Ghim, Y. S., Song, C. H., and Yoon, S.-C.: Aerosol properties at Gosan in Korea during two pollution episodes caused by contrasting weather conditions, *Asia-Pacific, J. Atmos. Sci.*, 48, 25–33, doi:10.1007/s13143-012-0003-9, 2012.
- KMOE (Ministry of Environment, Korea): Annual report of ambient air quality in Korea, 2011, 11-1480523-000198-10, National Institute of Environmental Research, Environmental Research Complex, Incheon, available at: <http://webbook.me.go.kr/DLi-File/091/012/5515496.PDF> (last access: 18 June 2014), 2012 (in Korean).
- KMOE (Ministry of Environment, Korea): Air pollutants emission (1999–2010), 11-1480523-001377-01, National Institute of Environmental Research, Environmental Research Complex, In-

- cheon, available at: <http://webbook.me.go.kr/DLi-File/NIER/09/018/5553596.pdf>, (last access: 18 June 2014), 2013 (in Korean).
- Lei, H., Wuebbles, D. J., Liang, X.-Z., and Olsen, S.: Domestic versus international contributions on 2050 ozone air quality: How much is convertible by regional control?, *Atmos. Environ.*, 68, 315–325, doi:10.1016/j.atmosenv.2012.12.002, 2013.
- Lei, H. and Wang, J. X. L.: Sensitivities of NO_x transformation and the effects on surface ozone and nitrate, *Atmos. Chem. Phys.*, 14, 1385–1396, doi:10.5194/acp-14-1385-2014, 2014.
- Levy, H., Mahlman, J., Moxim, W. J., and Liu, S.: Tropospheric ozone: the role of transport, *J. Geophys. Res.*, 90, 3753–3772, doi:10.1029/JD090iD02p03753, 1985.
- Levy, J. I., Chemerynski, S. M., and Sarnat, J. A.: Ozone exposure and mortality: an empiric Bayes meta-regression analysis, *Epidemiology*, 16, 458–468, doi:10.1097/01.ede.0000165820.08301.b3, 2005.
- Lin, C. Y. C., Jacob, D. J., and Fiore, A. M.: Trends in exceedances of the ozone air quality standard in the continental United States, 1980–1998, *Atmos. Environ.*, 35, 3217–3228, doi:10.1016/S1352-2310(01)00152-2, 2001.
- Lin, J.-T., Patten, K. O., Hayhoe, K., Liang, X.-Z., and Wuebbles, D. J.: Effects of future climate and biogenic emissions changes on surface ozone over the United States and China, *J. Appl. Meteorol. Clim.*, 47, 1888–1909, doi:10.1175/2007JAMC1681.1, 2008.
- Liu, S. C., Trainer, M., Fehsenfeld, F. C., Parrish, D. D., Williams, E. J., Fahey, D. W., Hübler, G., and Murphy, P. C.: Ozone production in the rural troposphere and the implications for regional and global ozone distributions, *J. Geophys. Res.*, 92, D4, 4191–4207, doi:10.1029/JD092iD04p04191, 1987.
- Logan, J. A.: Tropospheric ozone: seasonal behavior, trends and anthropogenic influence, *J. Geophys. Res.*, 90, 463–482, doi:10.1029/JD090iD06p10463, 1985.
- Lu, H. C. and Chang, T. S.: Meteorologically adjusted trends of daily maximum ozone concentrations in Taipei, Taiwan, *Atmos. Environ.*, 39, 6491–6501, doi:10.1016/j.atmosenv.2005.06.007, 2005.
- Lu, G. Y. and Wong, D. W.: An adaptive inverse-distance weighting spatial interpolation technique, *Comput. Geosci.*, 34, 1044–1055, doi:10.1016/j.cageo.2007.07.010, 2008.
- Mickley, L. J., Jacob, D. J., and Field, B. D.: Climate response to the increase in tropospheric ozone since preindustrial times: A comparison between ozone and equivalent CO₂ forcings, *J. Geophys. Res.*, 109, D05106, doi:10.1029/2003JD003653, 2004.
- Milanchus, M. L., Rao, S. T., and Zurbenko, I. G.: Evaluating the effectiveness of ozone management efforts in the presence of meteorological variability, *J. Air Waste Manage.*, 48, 201–215, doi:10.1080/10473289.1998.10463673, 1998.
- Nagashima, T., Ohara, T., Sudo, K., and Akimoto, H.: The relative importance of various source regions on East Asian surface ozone, *Atmos. Chem. Phys.*, 10, 11305–11322, doi:10.5194/acp-10-11305-2010, 2010.
- Oh, I. B., Kim, Y. K., Lee, H. W., and Kim, C. H.: An observational and numerical study of the effects of the late sea breeze on ozone distributions in the Busan metropolitan area, Korea, *Atmos. Environ.*, 40, 1284–1298, doi:10.1016/j.atmosenv.2005.10.049, 2006.
- Oh, I. B., Kim, Y. K., Hwang, M. K., Kim, C. H., Kim, S., and Song, S. K.: Elevated ozone layers over the Seoul Metropolitan Region in Korea: Evidence for long-range ozone transport from eastern China and its contribution to surface concentrations, *J. Appl. Meteorol. Clim.*, 49, 203–220, doi:10.1175/2009JAMC2213.1, 2010.
- Olszyna, K. J., Luria, M., and Meagher, J. F.: The correlation of temperature and rural ozone levels in southeastern U.S.A., *Atmos. Environ.*, 31, 3011–3022, doi:10.1016/S1352-2310(97)00097-6, 1997.
- Oltmans, S. J., Lefohn, A. S., Scheel, H. E., Harris, J. M., Levy II, H., Galbally, I. E., Brunke, E.-G., Meyer, C. P., Lathrop, J. A., Johnson, B. J., Shadwick, D. S., Cuevas, E., Schmidlin, F. J., Tarasick, D. W., Claude, H., Kerr, J. B., Uchino, O., and Mohnen, V.: Trends of ozone in the troposphere, *Geophys. Res. Lett.*, 25, 139–142, doi:10.1029/97GL03505, 1998.
- Oltmans, S. J., Lefohn, A. S., Harris, J. M., Galbally, I., Scheel, H. E., Bodeker, G., Brunke, E., Claude, H., Tarasick, D., Johnson, B. J., Simmonds, P., Shadwick, D., Anlauf, K., Hayden, K., Schmidlin, F., Fujimoto, T., Akagi, K., Meyer, C., Nichol, S., Davies, J., Redondas, A., and Cuevas, E.: Long-term changes in tropospheric ozone, *Atmos. Environ.*, 40, 3156–3173, doi:10.1016/j.atmosenv.2006.01.029, 2006.
- Oltmans, S. J., Lefohn, A. S., Shadwick, D., Harris, J. M., Scheel, H. E., Galbally, I., Tarasick, D. W., Johnson, B. J., Brunke, E.-G., Claude, H., Zeng, G., Nichol, S., Schmidlin, F., Davies, J., Cuevas, E., Redondas, A., Naoe, H., Nakano, T., and Kawasato, T.: Recent tropospheric ozone changes – A pattern dominated by slow or no growth, *Atmos. Environ.*, 67, 331–351, doi:10.1016/j.atmosenv.2012.10.057, 2013.
- Ordóñez, C., Mathis, H., Furger, M., Henne, S., Hüglin, C., Staehelin, J., and Prévôt, A. S. H.: Changes of daily surface ozone maxima in Switzerland in all seasons from 1992 to 2002 and discussion of summer 2003, *Atmos. Chem. Phys.*, 5, 1187–1203, doi:10.5194/acp-5-1187-2005, 2005.
- Racherla, P. N. and Adams, P. J.: Sensitivity of global tropospheric ozone and fine particulate matter concentrations to climate change, *J. Geophys. Res.*, 111, D24103, doi:10.1029/2005JD006939, 2006.
- Rao, S. T. and Zurbenko, I. G.: Detecting and tracking changes in ozone air quality, *J. Air Waste Manage.*, 44, 1089–1092, doi:10.1080/10473289.1994.10467303, 1994.
- Rao, S. T., Zalewsky, E., and Zurbenko, I. G.: Determining temporal and spatial variations in ozone air quality, *J. Air Waste Manage.*, 45, 57–61, doi:10.1080/10473289.1995.10467342, 1995.
- Rao, S. T., Zurbenko, I. G., Neagu, R., Porter, P. S., Ku, J. Y., and Henry, R. F.: Space and time scales in ambient ozone data, *B. Am. Meteorol. Soc.*, 78, 2153–2166, doi:10.1175/1520-0477(1997)078<2153:SATSIA>2.0.CO;2, 1997.
- Rasmussen, D. J., Fiore, A. M., Naik, V., Horowitz, L. W., McGinnis, S. J., and Schultz, M. G.: Surface ozone-temperature relationships in the eastern US: A monthly climatology for evaluating chemistry-climate models, *Atmos. Environ.*, 47, 142–153, doi:10.1016/j.atmosenv.2011.11.021, 2012.
- Shin, H. J., Cho, K. M., Han, J. S., Kim, J. S., and Kim, Y. P.: The effects of precursor emission and background concentration changes on the surface ozone concentration over Korea, *Aerosol Air Qual. Res.*, 12, 93–103, doi:10.4209/aaqr.2011.09.0141, 2012.
- Sillman, S. and Samson, P. J.: Impact of temperature on oxidant photochemistry in urban, polluted rural and re-

- mote environments, *J. Geophys. Res.*, 100, 11497–11508, doi:10.1029/94JD02146, 1995.
- Tang, G., Wang, Y., Xin, J., and Ren, X.: Surface ozone trend details and interpretations in Beijing, 2001–2006, *Atmos. Chem. Phys.*, 9, 8813–8823, doi:10.5194/acp-9-8813-2009, 2009.
- Tanimoto, H., Sawa, Y., Matsueda, H., Uno, I., Ohara, T., Yamaji, K., Kurokawa, J., and Yonemura, S.: Significant latitudinal gradient in the surface ozone spring maximum over East Asia, *Geophys. Res. Lett.*, 32, L21805, doi:10.1029/2005GL023514, 2005.
- Tanimoto, H., Ohara, T., and Uno, I.: Asian anthropogenic emissions and decadal trends in springtime tropospheric ozone over Japan: 1998–2007, *Geophys. Res. Lett.*, 36, L23802, doi:10.1029/2009GL041382, 2009.
- Thompson, M. L., Reynolds, J. R., Cox, L. H., Guttorp, P., and Sampson, P. D.: A review of statistical methods for the meteorological adjustment of tropospheric ozone, *Atmos. Environ.*, 35, 617–630, doi:10.1016/S1352-2310(00)00261-2, 2001.
- Tilmes, S. and Zimmermann, J.: Investigation on the spatial scales of the variability in measured near-ground ozone mixing ratios, *Geophys. Res. Lett.*, 25, 3827–3830, doi:10.1029/1998GL900034, 1998.
- Tsakiri, K. G. and Zurbenko, I. G.: Prediction of ozone concentrations using atmospheric variables, *Air Quality, Atmosphere & Health*, 4, 111–120, doi:10.1007/s11869-010-0084-5, 2011.
- Vingarzan, R.: A review of surface ozone background levels and trends, *Atmos. Environ.*, 38, 3431–3442, doi:10.1016/j.atmosenv.2004.03.030, 2004.
- Wang, T., Wei, X. L., Ding, A. J., Poon, C. N., Lam, K. S., Li, Y. S., Chan, L. Y., and Anson, M.: Increasing surface ozone concentrations in the background atmosphere of Southern China, 1994–2007, *Atmos. Chem. Phys.*, 9, 6217–6227, doi:10.5194/acp-9-6217-2009, 2009.
- Wang, X. and Mauzerall, D. L.: Characterizing distributions of surface ozone and its impact on grain production in China, Japan and South Korea: 1990 and 2020, *Atmos. Environ.*, 38, 4383–4402, doi:10.1016/j.atmosenv.2004.03.067, 2004.
- Wang, Y., Konopka, P., Liu, Y., Chen, H., Müller, R., Plöger, F., Riese, M., Cai, Z., and Lü, D.: Tropospheric ozone trend over Beijing from 2002–2010: ozonesonde measurements and modeling analysis, *Atmos. Chem. Phys.*, 12, 8389–8399, doi:10.5194/acp-12-8389-2012, 2012.
- Wise, E. K. and Comrie, A. C.: Extending the Kolmogorov-Zurbenko filter: Application to ozone, particulate matter, and meteorological trends, *J. Air Waste Manage.*, 55, 1208–1216, doi:10.1080/10473289.2005.10464718, 2005.
- Zhao, B., Wang, S. X., Liu, H., Xu, J. Y., Fu, K., Klimont, Z., Hao, J. M., He, K. B., Cofala, J., and Amann, M.: NO_x emissions in China: historical trends and future perspectives, *Atmos. Chem. Phys.*, 13, 9869–9897, doi:10.5194/acp-13-9869-2013, 2013.